This is a preprint, the final version is subject to change, of the American Mineralogist (MSA)
Cite as Authors (Year) Title. American Mineralogist, in press.
(DOI will not work until issue is live.) DOI: http://dx.doi.org/10.2138/am-2016-5538

Nickel – Cobalt Contents of Olivine Record Origins of Mantle Peridotite and Related Rocks

CLAUDE HERZBERG[1,*], CHRISTOPHER VIDITO[1] AND NATALIE A. STARKEY[2]

[1]Department of Earth and Planetary Sciences, Rutgers University, 610 Taylor Road, Piscataway NJ 08854, USA

[2]Planetary and Space Sciences, The Open University, Walton Hall, Milton Keynes, MK7 6AA, UK

Submitted to the American Mineralogist, August 19, 2015

Revision 2 submitted: April, 2016

Word count: 13789

E-mail: herzberg@rci.rutgers.edu

ABSTRACT

Olivine is distinguished from all other minerals in providing a remarkable chemical narrative about magmatic processes that occurred in Earth's crust, mantle, and core over the entire age of Earth history. Olivines in mantle peridotite have Ni contents and Mg numbers that were largely produced by equilibrium crystallization in an early turbulently convecting magma ocean; subsequent stages of partial melting operated to slightly elevate Ni and Mg number in residual olivines. Olivines from Archean komatiites from the Abitibi greenstone belt have Ni contents and Mg numbers that are consistent with an extensively melted peridotite source at great depths in the mantle. Olivines from basaltic oceanic crust, the Icelandic mantle plume and other Phanerozoic occurrences have compositions that record magma chamber crystallization, recharge, mixing and partial melting. Olivines from the present-day Icelandic mantle plume have compositions that are consistent the melting of a peridotite source; unlike Hawaii, the melting of recycled crust as a distinct pyroxenite lithology is not evident in the olivine chemistry of Iceland. Paleocene picrites from Baffin Island and West Greenland from the ancient Icelandic plume have olivines with Ni contents that are consistent with either Ni-rich peridotite that formed by core-mantle interaction or by low pressure crystallization of hot and deep magmas. In general, hot magma oceans, mantle plumes, and ambient mantle magmatism form in ways that are captured by the compositions of the olivine crystals that they contain.

INTRODUCTION

Olivine crystals in andesites, basalts, picritic melts, komatiites and mantle peridotite have Ni contents that range from about 1000 to 5000 ppm (Sobolev et al. 2007; Straub et al. 2008; Herzberg et al. 2013). This variability is a mineralogical record of magmatic origins. Nickel is no different from any other element in having abundance levels that depend on how it is partitioned amongst phases, processes such as mixing and melt-rock reaction, T-P conditions of partial crystallization and melting, in addition to the Ni contents of the sources that undergo melting. But what distinguishes nickel is that it is concentrated in olivine relative to the magmas from which it crystallizes (Hart and Davis 1978; Beattie et al. 1991; Matzen et al. 2013), and there is an abundance of data because it is easy to analyze. The problem is how to reliably extract information about origin from the Ni contents of olivine. We show that olivine chemistry provides a remarkable mineralogical narrative about magmatic processes in Earth's crust, mantle, and possibly core over the entire age of the Earth.

The narrative that olivine provides relies heavily on understanding how Ni is partitioned between olivine and liquid (i.e., $D_{Ni}^{Ol/L}$), which depends on temperature, pressure, and composition of the melt (Hart and Davis 1978; Beattie et al. 1991; Wang and Gaetani 2008; Filiberto et al. 2009; Li and Ripley 2010; Putirka et al. 2011; Niu et al. 2011; Matzen et al. 2013). $D_{Ni}^{Ol/L}$ decreases with increasing MgO content of the melt. But as increasing temperatures and pressures of melting yield melts with higher MgO contents (O'Hara 1968; Herzberg et al. 2007), it can be difficult to resolve the separate temperature (T)-pressure (P)- and composition (X) effects. This problem has given rise to a plethora of parameterization models of experimental data that calibrate $D_{Ni}^{Ol/L}$ as a function of T-P-X. It is an important problem to resolve because elevated Ni contents of olivine phenocrysts have been used to infer either pyroxenite melting in the source (Sobolev et al. 2005; 2007; Herzberg 2011), or elevated temperatures and pressures of melting of a peridotite source (Li and Ripley 2010; Niu et al. 2011; Putirka et al. 2011; Matzen et al. 2013).

We assume that nickel is partitioned between olivine and liquid as described by the empirical Beattie-Jones model, first formulated by Jones (1984) and later calibrated by Beattie et al. (1991). This model requires no independently adjustable temperature and pressure terms to understand how Ni is partitioned between olivine and melt. We discuss the advantages and limitations of this model, and compare it with the model of Matzen et al. (2013), which has the advantage that it is a thermodynamic parameterization of experimental data. The Beattie-Jones model is used in conjunction with an Fe-Mg partitioning parameterization of experimental data for olivine and melt (Toplis 2005; Herzberg and O'Hara 2002) to fully describe a forward model of the compositions of peridotite partial melts and the olivines from which they crystallize. It is shown that this olivine model provides an excellent description of measured olivines with relatively low Ni contents (i.e., $< \sim 3500$ ppm), and it can deepen our understanding of the origin of mantle peridotite, Archean komatiites, and Phanerozoic magmatism from oceanic spreading centers and mantle plumes.

COMPUTATIONAL METHOD

The method for calculating model olivine Ni compositions was given elsewhere (Herzberg and O'Hara 2002; Herzberg 2011) and is here developed and extended to include cobalt. Primary magma compositions are calculated first, followed by the olivines that they crystallize. We also examine the effects of fractional crystallization on modifying primary magmas, and provide examples of olivines that are expected to crystallize along a liquid line of descent; such olivine compositions have been appropriately termed "crystal line of descent", or CLD (Putirka et al. 2011).

The compositions of Ni in liquids extracted from dunite [L + Ol] and harzburgite [L + Ol + Opx] residues are obtained from mass balance solutions to the equation for accumulated fractional melting:

$$C_L = C_o\,[1 - (1-F)^{1/D}\,]/F \qquad (1)$$

where C_L = weight % NiO in the liquid (primary magma), C_o = initial NiO in the peridotite source composition, F = melt fraction, and D is the bulk distribution coefficient. This is suitable for most geological occurrences because melts drain by buoyant porous flow from their sources at low melt fractions (Ahern and Turcotte 1979; McKenzie 1984). However, we also consider batch melting equation:

$$C_L = C_o/(F(1-D) + D) \qquad (2)$$

which is appropriate for understanding high pressure experiments on KLB-1 (Herzberg and Zhang 1996), and we argue that it may have been important in the crystallization of Earth's magma ocean.

The Beattie-Jones model has been assumed for computing the compositions of olivine in equilibrium with a liquid of a known composition. The liquid composition in weight % oxides is first recalculated to mole % oxides on a mono-cation basis (i.e., MgO, NiO, $AlO_{1.5}$, $NaO_{0.5}$, etc), and the compositions of olivine are computed using the molar percent partition coefficients:

$$D_i^{Ol/L} = X_i^{Ol} / X_i^{L} \qquad (3)$$

where X_i refers to the mole fraction of oxide component i in liquid (L) and olivine (Ol). And in equations (1) and (2), the bulk distribution coefficient D is equal to $D_i^{Ol/L}$ and $D_i^{Opx/L}$ weighted according to the mass fractions of olivine and orthopyroxene that participate in melting, where $D_{NiO}^{Opx/L}$ and $D_{CoO}^{Opx/L}$ are from Beattie et al. (1991).

In the Beattie-Jones model, D_i depends on the partitioning of MgO between mineral and liquid. Based on an existing database at the time, Beattie et al. (1991) parameterized the experiments with the simple linear equations:

$$D_{NiO}^{Ol/L} = 3.346\, D_{MgO}^{Ol/L} - 3.665 \qquad (4)$$

and:

$$D_{CoO}^{Ol/L} = 0.786\ D_{MgO}^{Ol/L} - 0.385 \quad (5)$$

In equations (4) and (5):

$$D_{MgO}^{OL} = MgO^{Ol}/MgO^{L} \quad (6)$$

In these equations, the partitioning of Ni depends critically on the MgO content of the magma, which we explore from solidus to liquidus melting conditions for fertile peridotite. Experimental data of Walter (1998) on peridotite source KR4003 were used for much of the petrological modeling (Herzberg and O'Hara 2002). KR4003 contains 38.12% MgO (Herzberg and O'Hara 2002; Herzberg and Asimow 2015), slightly more depleted than the model pyrolitic mantle of McDonough and Sun (1995). Although KR4003 was reported to contain 0.24% NiO (Walter 1998), we assume that it contains the canonical value of 0.25% NiO (i.e., 1964 ppm; McDonough and Sun 1995). The major element geochemistry of model primary magmas for KR4004 has been given previously (Herzberg and O'Hara 2002; Herzberg 2004; Herzberg and Asimow 2015).

It is quite remarkable that the Beattie et al. (1991) parameterization performs extremely well in describing more recently acquired experimental data discussed below. However, we have chosen not to update the parameterized constants in equations (4) and (5) because the Ni and Co contents of computed olivines and liquids are not greatly improved, and they are well within the uncertainties discussed below.

The Ni contents for near–solidus melts were calculated from the MgO contents of near–solidus melts (Herzberg and O'Hara 2002) together with a solidus olivine composition having 0.365% NiO, which is characteristic of high precision analysis of olivines having an Mg number of 89.5 (Herzberg et al. 2013; see below). In a similar way, we constrain the Co content of near-solidus melts using olivine with 0.0172% CoO as we report below for high precision electron microprobe analysis of San Carlos olivine. It will be shown below that Ni contents of solidus melts are similar to or slightly higher than those for L+Ol and L+Ol+Opx, placing confidence in all interpolation possibilities for spinel and garnet peridotite.

The Mg number (i.e., 100MgO/(MgO + FeO); cationic) of olivine is computed using the partitioning of Fe and Mg between olivine and liquid:

$$K_D^{Ol/L}{}_{FeO/MgO} = D_{FeO}^{Ol/L} / D_{MgO}^{Ol/L} \quad (7)$$

For crystallization of olivine at near-surface conditions, we use the thermodynamic parameterization of Toplis (2005), wherein K_D is typically ~ 0.30 for mid ocean ridge-like basalts, as originally constrained by Roeder and Emslie (1970). However, K_D is elevated at high pressures in the melting region, and in this case we use the parameterization of Herzberg and O'Hara (2002) for batch and accumulated fractional melting; application of this model to the

high pressure experimental results of Walter (1998) yields K_D that is very similar to that obtained from the Toplis (2005) model.

COMPUTATIONAL UNCERTAINTIES

The advantage of the Beattie-Jones model is that it requires no independently adjustable temperature and pressure terms to understand how Ni is partitioned between olivine and melt; this arises because elevated temperatures and pressures of melting typically result in elevated MgO contents of primary magmas of mantle peridotite, and the T-P variability is captured to a large extent by the $D_{MgO}^{Ol/L}$ term. A disadvantage is that the Beattie-Jones model is not grounded in a thermodynamic analysis, and there may be situations in nature wherein variations in $D_{NiO}^{Ol/L}$ are not adequately captured by $D_{MgO}^{Ol/L}$ in the parameterized experimental database. In contrast, the model of Matzen et al. (2013) describes $D_{Ni}^{Ol/L}$ with independently adjustable T-P-X terms in a Gibbs energy equation and, in principle, it should be a more robust method. However, a disadvantage of the Matzen et al. (2013) model is that it requires an understanding of the T-P conditions of melting and crystallization. While improved constraints are now becoming available (e.g., Ghiorso and Sack 1995; Herzberg and Asimow 2015; Hole and Millet, 2016), the absolute T and P melting conditions are models that add a new layer of uncertainty. And in the case of magma ocean formation considered below, the T-P conditions of melting are not well known, and it is under these circumstances where the Beattie-Johns model is particularly useful.

In a previous paper (Herzberg et al. 2014), it was suggested that the Beattie-Jones model was more accurate than the Matzen et al. (2013) model because it provided the minimum absolute root mean square error (A RMSE). This analysis was based on comparison of the two different models based on the absolute difference between experimental and model values of $D_{NiO}^{Ol/L}$ (i.e., D Ni XP - D Ni Model) so that the absolute mean square error is:

$$\text{A RMSE} = (\Sigma(\text{D Ni XP} - \text{D Ni Model})^2/\text{N})^{0.5} \quad (8)$$

where D Ni XP is the experimentally measure value of $D_{NiO}^{Ol/L}$ and D Ni Model is $D_{NiO}^{Ol/L}$ predicted by the model. The problem with this approach is that the Matzen et al. (2013) model $D_{NiO}^{Ol/L}$ values as expressed on a molar basis are higher for individual experiments than those of Beattie-Jones, which gives rise to an artificially high A RMSE. A better way to compare partitioning different models is to use the *relative* difference between experimental and model values of $D_{NiO}^{Ol/L}$ (i.e., D Ni XP - D Ni Model)/D Ni XP), so that the relative root mean square error is:

$$\text{R RMSE} = ((\text{D Ni XP} - \text{D Ni Model})/\text{D Ni XP})^2/\text{N})^{0.5} \quad (9)$$

Results are shown in Table A1 for various experimental databases. Matzen et al. (2013) critically evaluated the quality of the experimental database, and recommended that data of questionable quality be filtered. Using the filtered database A consisting of 325 experiments with and without FeO, the Matzen et al. (2013) model has a R RMSE = 0.21, and it is more accurate than the Beattie-Jones model with a R RMSE = 0.25. The experimental database

assembled by Herzberg et al. (2013) was unfiltered for data quality, but filtered to include data with FeO as being representative of basalts, picrites and komatiites in nature; data without FeO were excluded. This database (Herzberg et al. 2013) is archived in Table A2 of the Appendix, and was constructed from experimental data compiled by Li and Ripley (2010) to which the data of Matzen et al. (2010; 2013) were added. There are 284 experiments in Table A2, and Table A1 shows that the models of Matzen et al. (2013; R RMSE = 0.23) and Beattie-Jones (R RMSE = 0.21) are essentially of equal accuracy in describing these data. This is more easily visualized in Figures 1a and 1b. Moreover, Figure 1c shows that the Matzen et al. (2013) model description of the experiments is well captured by the Beattie-Jones model.

Both olivine/melt NiO partitioning models describe equally well (i.e., R RMSE = 0.21) the database A of Matzen et al. (2013) that was filtered for quality and which was restricted to FeO-bearing samples only (Table A1). It is not clear why FeO-free experiments yield a less accurate Beattie-Jones model. However, we focus on understanding the relationship between olivine Mg number (i.e., mole% 100MgO/(MgO + FeO)) and Ni content of naturally-occurring olivines, and the Beattie-Jones model is clearly justified. As shown in Figure 1 and Table A1, there is no intrinsic disadvantage of Beattie-Jones compared with Matzen et al. (2013) model, despite the fact that it is not rooted in a thermodynamic parameterization. However, we acknowledge that while the Beattie-Jones model provides an excellent description of many olivine occurrences discussed below, it may fail in situations where melting and crystallization in nature operate outside the experimental calibration bounds. In a section that follows, we show that both nickel partitioning models do a good job of describing the Ni contents of olivines from the Paleocene picrites from West Greenland and Baffin Island.

NICKEL CONTENTS OF OLIVINE AND MANTLE MELTS OF A PERIDOTITE SOURCE

Model Results

The Ni contents of near–solidus primary magmas are only slightly higher than those of primary magmas for L+Ol and L+Ol+Opx assemblages, and the full range of possibilities are shown in Figure 2a for batch melting of fertile peridotite KR4003; however, this small difference in melt Ni content is magnified by the Ni contents of coexisting olivines, which can show a range of values at constant MgO and Mg-number. The compositions of olivine coexisting with liquids for which olivine is the only crystalline phase (L+Ol) are shown as blue tie-lines. There is considerable rotation of the tie lines through the bulk composition that illustrates mostly compatible behavior of Ni in olivine. However, at MgO in the ~ 36 to 38% range the Ni content of model olivine is less than the Ni content of these high MgO melts, demonstrating incompatible behavior. As temperatures decrease from the liquidus to the solidus, the large drop in Ni in melts is mass balanced by a large Ni gain in olivine (Figure 2a).

For accumulated fractional melting of fertile peridotite, the Ni content of a primary magma is:

$$\text{Ni (ppm)} = 21.6\text{MgO} - 0.32\text{MgO}^2 + 0.051\text{MgO}^3 \quad (10)$$

for MgO contents < 27% (Herzberg 2011). The Ni contents of accumulated fractional melts of fertile peridotite are slightly higher than those of batch melts at any specific MgO content, and they are similar to the Ni contents of melts on the solidus (Figure 2b). Importantly, for any specific mode of melting and melt MgO contents < 27%, the Ni content of a primary melt is essentially identical for both fertile and depleted peridotite sources (Figure 2b).

The Ni contents of olivine in equilibrium with primary magmas of fertile peridotite are given in Figure 3 at mantle pressures appropriate to partial melting, which typically range from ~ 2 to 6 GPa for Phanerozoic magmas (Herzberg and Asimow 2015). Slight elevations in Ni for accumulated fractional melts relative to batch melts (Figure 2b) are reflected in their slightly higher olivine Ni contents (Figure 3a). It is important to note, however, that a computed aggregate fractional melt is not in equilibrium with its residue and residual olivine; only the final drop of liquid extracted is in equilibrium with the residue (Herzberg 2004). Nevertheless, it will be shown below that the assumption of equilibrium is a good approximation.

Our analysis of olivines of primary magmas of a peridotite source always show an maximum of Ni content with increasing melt fraction (F; Figure 3a). For the case of accumulated fractional melting, the Ni content of olivine is ~ 2860 ppm at the solidus, increasing to a maximum of 3100 ppm at F = ~ 0.5, and then decreasing by almost half to 1600 ppm at F = 1. The large drop in olivine Ni content is nothing more than a mass balance requirement of the large increase in melt Ni content from the solidus to the liquidus (Figure 2a). Our model differs fundamentally from that reported by Straub et al. (2008), wherein their Ni contents increase continuously with increasing degree of melting (Figure 3a). As a critical test, we compare our model olivine compositions for batch melting at high pressures with olivine compositions measured from experiments on peridotite KLB-1 (Zhang and Herzberg 1994; Herzberg and Zhang 1996). Results are compared with that of Straub et al. (2008) and, although this model is for fractional melting, it will not differ significantly from our batch melting model.

The experimental olivines are distributed between the solidus and liquidus in experiments that were conducted in a temperature gradient on peridotite KLB-1, which has 0.25% NiO (see Figure 4 in Zhang and Herzberg 1994). Only a few representative olivines were reported by Herzberg and Zhang (1996), and we include the full dataset in Table A3 of the Appendix. There is liquid migration toward the hot spot in a temperature gradient by the solution and precipitation of crystalline phases dominated by olivine (e.g., Lesher and Walker 1988; Zhang and Herzberg 1994). Expulsion of low degree melts from near the solidus and toward the liquidus near the hotspot results in mixed melts, and there is a continuum of olivine compositions in equilibrium with these melts (Figure 3b). Notably, experimental olivines from melts near the liquidus have the lowest Ni contents, about 1600 ppm Ni, and maximum Ni contents of about 3100 ppm (Figure 3b). We have not examined the possibility that the low olivine Ni contents were compromised by Ni loss to rhenium containers; however significant Ni loss is not likely because there is good mass balance in Ni between near liquidus olivine and liquid compositions with respect to 0.25% for the bulk KLB-1 composition, within the reported uncertainties (Herzberg and Zhang 1996). This provides experimental confirmation of our model olivine compositions

calculated from Beattie-Jones, Toplis, and Herzberg-O'Hara parameterizations of experimental data. Low Ni olivine contents near the liquidus illustrate the incompatible nature of Ni in olivine with respect to near-total melts of mantle peridotite.

Olivine in Mantle Peridotite

The evidence presented in Figure 4 suggests that olivines in mantle peridotite could have been in equilibrium with primary melts that formed by either batch or accumulated fractional melting. This conclusion is based on the excellent match between calculated olivine compositions for our assumed peridotite having 0.25% NiO (McDonough and Sun 1995) and those of 215 olivine grains in mantle peridotites from a wide range of tectonic environments that have been measured by high precision electron microprobe analysis (Herzberg et al. 2013). These natural olivines contain 2800 to 3100 ppm Ni, and Mg numbers in the 89.5 to 92.0 range (Figure 4a), and there is a positive relationship between Ni and Mg number (i.e., $\delta Ni/\delta Mg$ number = 68), which is captured in the computed olivine compositions. Olivines from peridotite residues that have Ni compositions outside the bounds shown in Figure 4a have been reported (e.g., Doucet et al. 2012), indicating the operation of second stage processes such as interaction with sulfide (Barnes et al. 2013).

If mantle peridotite is the solidification product of an early magma ocean (Herzberg and O'Hara 1985; Melosh 1990; Tonks and Melosh 1993; Walter and Trønnes 2004; Elkins-Tanton 2012; Carlson et al. 2014) then the evidence from olivine indicates that it melted and crystallized with little or no removal of olivine (i.e., equilibrium/batch melting and crystallization; Figure 4b). The liquidus temperature of a totally melted fertile peridotite composition similar to KR4003 at 1 atmosphere is ~ 1700°C, and > 2000°C at P > 7 GPa (Herzberg and Asimow 2015). The liquidus olivine to crystallize from this magma ocean composition would have an Mg number of 96 and a Ni content of 1600 ppm (Figure 4b). Olivine compositions of equilibrium (batch) crystallization would equilibrate to lower Mg numbers and higher Ni contents, reaching a maximum of about 3000 ppm Ni after about 70% crystallization. At total solidification, the fertile peridotite would have olivine containing 2860 ppm Ni and an Mg number of 89.5, similar to those that have been measured (Figure 4b; Herzberg et al. 2013); olivines with higher Mg numbers likely formed in a second stage as residual olivines after melt extraction (Figure 4a).

Formation of mantle peridotite by perfect removal or fractional crystallization of olivine in a terrestrial magma ocean is not plausible unless there is an error in our assumed peridotite composition. This process would form olivines with an array of compositions, many of which would have had much higher Ni contents than observed. The red curve in Figure 4b describes the olivine crystal line of descent that would result from 0 to 82% fractional crystallization of olivine from a totally melted peridotite. The calculation does not include the crystallization of pyroxenes, spinel and garnet, all of which would elevate the Ni contents of the magma ocean and its crystallizing olivines as indicated by the red arrow because Ni is more incompatible in these phases than olivine (Beattie et al. 1991; Herzberg et al. 2013); their inclusion would further magnify the misfit between the olivine-only CLD and observed mantle olivines. However, the slightly higher Ni contents of observed olivines relative to the equilibrium crystallization

situation (Figure 4b) might be accommodated by a small measure of fractional crystallization. That is, olivine may have maintained an equilibrium composition with its magma ocean owing to suspension as it crystallized, but it might not have been perfect owing to a small amount of removal somewhere. The petrological evidence for the dominant operation of equilibrium crystallization is consistent with convection velocities that were higher than settling velocities at relatively low pressures appropriate to olivine stability (Tonks and Melosh 1990; Solomatov 2015). Trace element and isotopic evidence indicate that fractional crystallization might have been more important in the lower mantle, involving perovskite and ferropericlase (Caro et al. 2005; Corgne et al. 2005; Labrosse et al. 2007; Rizzo et al. 2011; Puchtel et al. 2013). This might be manifest by lithological and geochemical heterogeneity at D" (Labrosse et al. 2007; Coltice et al. 2011), in contrast with the remainder of the mantle from which peridotite is sampled.

A corollary to the formation of Earth's mantle by equilibrium-dominated crystallization is that its magma ocean solidified to a peridotite mantle its own composition, with little or no basaltic type differentiates and dunite cumulates anywhere. This implies the Earth's surface was largely made of peridotite at some early stage, a conjecture that might be consistent with some magma ocean models that suggest the Earth cooled from a total melt to a complete solid in a short period of time, that is 10^6-10^7 years (Hamano et al. 2013; Elkins-Tanton 2008). However, these estimates are highly uncertain because there is currently no comprehensive physical model of magma ocean crystallization that considers the time scales of crystal nucleation, growth and separation from liquid (Solomatov 2015). Nevertheless, the evidence from the Ni content of olivine in mantle peridotite points to a major role for equilibrium crystallization in an early turbulently convecting magma ocean; subsequent stages of partial melting operated to slightly elevate Ni and Mg number in residual olivines. Uncertainties in the depths and temperatures of magma ocean melting and crystallization provide a good example of the utility of using the Beattie-Jones model for understanding the Ni content of olivine.

Olivine in Archean Komatiites

Archean-age komatiites from Alexo and Munro in the Abitibi greenstone belt have compositions that indicate extreme degrees of melting of a peridotite source. Petrological analysis indicates all crystalline phases were melted out except olivine (Herzberg 2004), and primary magma compositions have been estimated to have contained 26-30% MgO (Arndt et al. 2008; Herzberg 2011). The major element geochemistry of Alexo and Munro komatiites is consistent with accumulated fractional melting (see Figure 11 in Herzberg 2004).

Olivine compositions from Alexo and Munro komatiites are shown in Figure 5 together with those that have been modeled for olivines that crystallize at the surface from primary accumulated fractional melts of a peridotite source (Herzberg 2011). As shown more clearly below and in Figure 6, model olivines of primary magmas that crystallize at the surface have slightly higher Mg numbers than do those that crystallize in the mantle. Many olivines from Alexo contain about 3300 ppm Ni and Mg numbers of 94.5 (Sobolev et al. 2007), in good agreement with those expected to crystallize from a primary magma having 30% MgO; other olivines are more consistent with 26% MgO. In some cases, observed olivines have Ni contents

that are up to ~ 500 ppm higher than those expected of primary magmas, and this might indicate a pyroxenite contribution to melting (Sobolev et al. 2007). However, the pyroxenite interpretation is not consistent with olivine Mn and Ca contents (Figure 7b in Herzberg 2011), indicating that the komatiites melted from a peridotite source that was free of recycled crust. Instead, Alexo and Munro olivines have Ni contents that are similar to model olivines produced by partial melting of a normal peridotite source having 1964 ppm Ni, followed by fractional crystallization of olivine. Importantly, calculated olivine crystal lines of descent capture the curvature to the Ni-Mg number systematics in measured olivines (Figure 5; Herzberg 2011). For example, fractional crystallization of olivine from a primary magma having 30% MgO would drive up the Ni content of olivine from 3040 to 3660 ppm (Figure 5). This unusual behavior contrasts with the more familiar drop in Ni along an olivine CLD as seen in Figure 6 for MORB primary magmas with lower MgO contents.

The volatile-free liquidus temperature of a primary magma having 30% MgO is 1600°C at 1 atmosphere, and > 1800°C at P > 5 GPa (Herzberg and Asimow 2015). Based on the phase diagram for KLB-1 (Herzberg and Zhang 1996), melting might have commenced in the lower mantle or transition zone, and may be consistent with mantle potential temperatures in the 1800 to 2000°C range (Herzberg et al. 2010; Putirka 2016). Archean komatiites have higher MgO contents than the more common contemporaneous basalts that melted from ambient mantle (Herzberg et al. 2010), consistent with a hot plume origin (e.g., Arndt et al. 2008; Herzberg et al. 2010). However, this conclusion assumes that volatile-free melting is valid. Evidence has been presented for a role played by CO_2 and H_2O in melting that produced the komatiites from Alexo and Pyke Hill (Sobolev et al. 2016), and there is ambiguity concerning the mantle potential temperature of the source (Herzberg 2015). Melting of peridotite that was carbonated will be extensive and highly productive owing to the effect of CO_2 in lowering the solidus temperature (Dasgupta 2013); unfortunately, the extent to which degassing has affected CO_2 and H_2O is not known (Herzberg 2015), and the depths of melting may have been located anywhere from the lower to the upper mantle. Uncertainties in the depths and temperatures of melting provide another good example of the advantage of using the Beattie-Jones model for understanding the nickel content of olivine.

Olivine from Mid-Ocean Ridge Basalts

New high precision electron microprobe data have been obtained on olivines from the Siqueiros fracture zone at the East Pacific Rise (Table A4) using analytical methods described in the Appendix. Results are shown in Figure 6 together with high precision data from the Southeast Indian Rise (Sobolev et al. 2007). The trend of olivine analyses matches reasonably well the computed CLD for a representative MORB primary melt composition from the Siqueiros fracture zone having 11.5% MgO (Herzberg and Asimow 2015). The most primitive olivines have Ni contents that trend towards 2900 ppm, similar to those of model olivines from primary magmas. Those olivines displaying low Ni contents relative to the CLD might indicate sequestration from a sulfide phase (Herzberg 2011); high Ni olivines might be attributed to magma chamber crystallization, recharge, mixing, and tapping (O'Hara 1977; Coogan and O'Hara 2002; O'Hara and Herzberg 2002; O'Neill and Jenner 2012). However, the overall good

agreement between observed and calculated olivine Ni contents indicates a robust computational method constructed from Beattie-Jones, Toplis, and Herzberg-O'Hara partitioning parameterizations. And the success of this model to mantle peridotite (Figure 4b; Ol liquidus T at 1 atmosphere = 1700°C), Archean komatiites (Figure 5), and present-day MORB (Figure 6; Ol liquidus T at 1 atmosphere = 1280°C) is a good illustration of its general applicability to an extremely wide range of temperature and pressure environments on Earth.

Olivine from Iceland: The Modern Icelandic Mantle Plume

Iceland is the modern expression of volcanism from a mantle plume that can be tracked back in time to its first eruption in the Paleocene (Saunders et al. 1997). Olivine compositions from Theistareykir volcano are shown in Figure 7, and they are representative of the full range of possibilities from other volcanoes on Iceland (Sobolev et al. 2007). There are two major populations of data. The first can be reasonably described by model olivines that crystallized for the equilibria L+Ol and L+Ol+Plag (Figure 7). The second olivine population has a lower Mg number at constant Ni content, and is roughly coincident with the curved red lines shown in Figure 7. These red lines represent olivines that crystallize from magmas that form by the mixing of the primary magma with derivative magmas along the LLD. This is a simulation of magma chamber crystallization, recharge, and mixing (O'Hara 1977) and it shares some similarities to those for MORB (O'Neill and Jenner 2012; Coogan and O'Hara 2015), Mangaia and Curacao picrites (Herzberg et al. 2014; Trela et al. 2015). Although the calculations were performed at 1 atmosphere, the effect of increasing the pressure to those expected in the deeper crust is to shift the Ni contents of olivines on the L+Ol+Plag+Cpx CLD, but this will not affect the mixing lines.

Figure 7 illustrates the very good agreement between observed and calculated olivine Ni contents using Beattie-Jones, Toplis, and Herzberg-O'Hara parameterizations. White circles are olivine compositions that have been calculated using the method of Matzen et al. (2013) for $D_{NiO}^{Ol/L}$ and with the assumption of 2975 ppm Ni in the peridotite source olivine (Figure 4). Matzen et al. (2013; 2016) have suggested that the Ni contents of olivine phenocrysts will be elevated for the condition of higher temperatures and pressures of magma generation in the mantle compared with the temperature of crystallization in the crust, a ΔT effect. This is shown in Figure 7 for melting pressures that range from 0 to 2.1 GPa. Indeed, the Matzen model is sensitive to assumptions concerning the conditions of melting. Flipping this around, there is great potential for using the Matzen method for independently estimating final pressures of melt segregation in the mantle. However, it is only for a melt segregation pressure of 0 GPa where there is excellent agreement with both observed and calculated olivines using the Beattie-Jones parameterization, an implausible result because melting must be deeper than the Icelandic crust, which is 25 to 40 km thick (Darbyshire et al., 2000). A melting pressure of 1.0 GPa yields a higher Matzen Ni content for olivine, but it is well within the uncertainty of the partitioning models. However, these Matzen pressures depend on the assumed Ni content of the olivine in the residual mantle. If we drop Ni from 2975 Ni to 2710 ppm, then a good match can be obtained with observed olivines at an assumed a pressure of 1.0 GPa below Iceland. Olivine in mantle

peridotite with 2710 ppm Ni is lower than the average of our high precision data and the expectation of 1964 ppm Ni in fertile peridotite (Figure 4), but it is a reasonable low Ni bound.

There are two important messages to be drawn from Figure 7. The first is that olivines from Iceland have Ni contents that are well described by model olivines expected by melting of a normal peridotite source having a canonical Ni content of 1964 ppm (McDonough and Sun 1995). Icelandic olivines do not have Ni contents in excess of 3000 ppm, differing from those observed from Hawaii and for which pyroxenite source melting has been inferred (e.g., Figure 7; Sobolev et al. 2007; Herzberg 2011); a peridotite source for Iceland inferred from Ni is also consistent with high Ca and Mn, and low Fe/Mn, in contrast with Hawaii (please see below; Herzberg et al. 2013). The second message is that inferences about source lithology can be compromised without due consideration given to magma chamber crystallization, recharge, and mixing. For example, the Theistareykir olivine population with low Mg number might be erroneously interpreted as requiring the involvement of a modest amount of pyroxenite as it is shifted in the direction towards Hawaii; but to reiterate, this is not consistent with a peridotite source as expressed by olivine phenocrysts having high Ca and Mn, and low Fe/Mn (see below).

We conclude that the evidence from olivine chemistry points to little or no role is played by recycled crust as a distinct lithology in the present-day Icelandic mantle plume. In contrast, the enriched and depleted geochemical variability (e.g., Fitton et al. 2003) was interpreted by Shorttle et al. (2014) as arising from the melting a lithologically heterogeneous source consisting of recycled crust imbedded in buoyant harzburgite. We suggest herein that another possibility might be a source that consists of harzburgite with variable amounts of recycled crust mixed in. It was noted previously that the Ni contents of primary melts (i.e., MgO < 27%) of peridotite having 38 to 42% MgO are essentially identical (Figure 2b), as will be the Ni contents of their crystallizing olivines. Therefore, olivine phenocryst chemistry cannot be used to distinguish a fertile peridotite source from a depleted harzburgitic source that had been variably refertilized by mixing moderate amounts of recycled crust.

Mantle plumes may be anchored at the edges of Large Low Shear Velocity Provinces on the core-mantle boundary (Burke et al. 2008), and LLSVPs may consist of ambient mantle mixed with recycled crust (Mulyukova et al. 2015), primordial mantle differentiates (Labrosse et al. 2007), or both. Recycled crust from the LLSVP was sampled by the Hawaiian mantle plume (Weis et al. 2011) which stretched it into filaments (Farnetani and Hofmann 2009), but it was not mixed or destroyed as a distinct pyroxenite lithology as indicated by high Ni olivine in Figure 7 (Sobolev et al. 2007; Herzberg 2011). From a petrological point of view, Iceland does not conform to this standard model as its olivine Ni contents are low and consistent with peridotite melting (Figure 7). Mangaia is another example, although in detail the olivine compositions differ from those of Iceland (Herzberg et al. 2014). The question is how exactly does recycled crust get mixed into its peridotite host? Destruction of recycled crust may occur by partial or total melting of the pyroxenite and injection of its silicic melts into the surrounding mantle peridotite, yielding a relatively refertilized peridotite (Yaxley and Green 1998). Such a source can have phantom-like properties in that its lithological identity as recycled crust can be destroyed while its trace element and isotope ratios are preserved in the refertilized peridotite (Herzberg et al. 2014). Whether pyroxenite is destroyed as in Iceland or preserved as in Hawaii

will depend on a potentially complex interplay amongst its mass relative to the peridotite host, the thermal properties of the mantle plume, and the thickness of the lithosphere. The signal of pyroxenite melting in olivine chemistry is likely to be stronger for mantle plumes that impact a thick lithosphere (Sobolev et al. 2007) because pyroxenite has a lower solidus temperature and higher melt productivity relative to peridotite (e.g., Morgan 2001; Pertermann and Hirschmann 2003; Ito and Mahoney 2005; Sobolev et al. 2007; Shorttle and Maclennan 2011). The present-day Icelandic mantle plume is only slightly cooler than Hawaiian plume (Herzberg and Asimow 2015), but it is coincident with the Mid Atlantic ridge; therefore, the Icelandic melting column is drawn closer to the surface relative to Hawaii, and there are increased opportunities for pyroxenite destruction and peridotite refertilization.

Olivine from the Paleocene Picrites of West Greenland (WG) and Baffin Island (BI): The Ancient Icelandic Mantle Plume

Paleocene picrites from West Greenland and Baffin Island were the first magmatic eruptions from the ancestral Icelandic mantle plume (Saunders et al. 1997), and they are notable in having the most primitive He, Pb and Nd isotopic compositions on Earth (Stuart et al. 2003; Starkey et al. 2009; Jackson et al. 2010). Inversion of the major elements indicate that they crystallized from high MgO lavas that were generated by a hot mantle plume source (Larsen and Pedersen 2000; Herzberg and O'Hara 2002; Herzberg and Gazel 2009; Hole and Millet 2016). The implication is that the ancestral Icelandic mantle plume sampled a primitive region of Earth's mantle.

Low and high precision data (Larsen and Pedersen 2000; Sobolev et al. 2007) show that olivines from WGBI lavas have Ni contents that are higher than those expected of melting of a peridotite source having a canonical Ni content of 1964 ppm (Herzberg et al. 2013). This result has been reproduced and illustrated again in Figure 8 with new high precision electron microprobe data that we report in Table A5 of the Appendix. The trend of WGBI olivines is not consistent with the expectations of a crystal line of descent involving L+Ol and L+Ol+Plag. Crystallization of clinopyroxene is indicated, followed by mixing with more primitive melts as for Theistareykir volcano. Importantly, the signal of clinopyroxene crystallization will be revealed in olivines with elevated Ni, but the rocks may contain no clinopyroxene as a phenocryst phase. Together with MORB (Figure 6), Mangaia (Herzberg et al. 2014), Curacao (Trela et al. 2015), and Theistareykir (Figure 7), olivine from West Greenland and Baffin Island is faithfully recording in its chemistry the widespread occurrence of magma chamber fractional crystallization, recharge, and mixing (O'Hara 1977; Coogan and O'Hara 2015; O'Hara and Herzberg 2002; O'Neill and Jenner 2012).

Some olivines from Baffin Island with Mg numbers in the 85-88 range have Ni contents that are similar to olivines that crystallized from mixed magmas of Theistareykir volcano; however, the same BI olivine population with Mg numbers > 90 is always higher in Ni by as much as 500 ppm in some cases, indicating a fundamental difference with respect to the modern Icelandic mantle plume. One possible explanation is that Ni is high in WGBI olivines because of the participation of recycled crust. However, while recycled crust is likely to be compositionally

heterogeneous (Herzberg 2011), olivines that crystallize from melts of a pyroxenite source commonly have low Ca and Mn contents, and elevated Fe/Mn; this signature can arise from retention of Ca and Mn in modally abundant residual clinopyroxene and garnet, respectively (Herzberg 2011). This is in contrast with olivines from WGBI that have Mn, Fe/Mn, and Ca contents similar to those of olivines in MORB (Herzberg et al. 2013), as is shown in Figure 9. Fe/Mn for olivines from WGBI and Theistareyker volcano are similar to those for MORB and model olivines expected of a peridotite source; they are also much lower than Fe/Mn of olivines from Hawaii for which a pyroxenite source has been interpreted (Sobolev et al. 2007; Herzberg 2011).

In general, olivines from West Greenland have slightly higher Ni contents than do those from Baffin Island (Figure 8). No correlation exists between excess Ni in olivine and the isotopic compositions of the lavas from which our olivine analyses were obtained (Starkey et al. 2009). The only correlation observed in trace element ratios is that West Greenland lavas generally have higher V/Sc than do Baffin Island lavas (Figure 10). This is based on histograms of V/Sc for West Greenland and Baffin island lavas (Larsen and Pedersen 2009; Lightfoot et al. 1997; Starkey et al. 2009) that have been filtered with Nd and Sr isotope ratios to exclude samples that had experienced crustal contamination (Larsen and Pedersen 2009). Increasing fO_2 increases V/Sc in melts of spinel and garnet peridotite (Lee et al. 2005), but the effect is greater for garnet peridotite (Mallmann and O'Neill 2009) at constant fO_2. This is consistent with petrological modeling that shows overlapping but generally greater depths of melting in the generation of West Greenland primary magmas compared with Baffin Island (Hole and Millett 2016).

The Beattie-Jones Ni partitioning model for a McDonough and Sun (1995) peridotite predicts olivines with lower Ni contents than those observed for WGBI, but the misfit is within the uncertainty of the model. Matzen et al. (2013; 2016) have suggested that Ni contents of olivine phenocrysts that crystallize at the surface will be elevated for hotter melts generated deeper in the mantle, the ΔT effect. This interpretation is consistent with higher Ni contents of WG olivines compared with BI olivines (Figure 8). Olivines represented by the white circles in Figure 8 have been calculated using the method of Matzen et al. (2013) for $D_{NiO}^{Ol/L}$ assuming an olivine Ni content of 2975 ppm Ni in the peridotite source (Figure 4), melting pressures that range from 2.8 to 2.1 GPa, and crystallization at the surface (see caption for details). The agreement with many WGBI olivines is very good for the high Ni population (Figure 8). Some of the low Ni BI olivine population is consistent with a Matzen melting pressure of 2.1 GPa; however, BI olivines with the lowest Ni contents would likely require unreasonably low pressures or Ni-depleted peridotite.

How do we explain Icelandic and WGBI olivines that have similar Fe/Mn (Figure 9) but different Ni contents (Figures 7, 8)? This paradox was explained by Paleocene picrites that melted from a nickel-rich peridotite source (Figure 8), Ni being high owing to interaction with the core (Herzberg et al. 2013). However, this interpretation is no longer unique because the Beattie-Jones $D_{NiO}^{Ol/L}$ model was assumed. In contrast, the nickel partitioning model of Matzen et al. (2013) is consistent with elevated Ni in olivine owing to deep and hot melting of normal mantle peridotite having the canonical 0.25% NiO (McDonough and Sun 1995) and containing

residual olivines with 2975 ppm Ni (Figures 4). The nickel-rich peridotite hypothesis (Herzberg et al., 2013) is now less secure, but Ni contents of olivine using the Matzen et al. (2013) method are sensitive to assumed T-P conditions of melting and Ni content of residual olivine. We caution, however, against over interpretation because the uncertainties in both Beattie-Jones and Matzen models are about the same (Figure 1; Table A1), and they propagate to significant uncertainties in the Ni content of olivine as shown in Figure 8. More work is needed to constrain the problem.

Olivine from Hawaii

Picrites from the West Greenland Vaigat Formation were proposed to have segregated below a thick 100-120 km continental lithosphere (Larsen and Pedersen 2000), consistent with model pressures reported by Hole and Millet (2016). These pressures are comparable to those below Hawaii (Li et al. 2000; 2004), and mantle potential temperatures for WG and Hawaii are are about the same (T_P = 1500-1600°C; Herzberg and Gazel 2009; Hole and Millet 2016). Therefore, it is expected that the model of Matzen et al. (2013; 2016) would predict olivine Ni contents from West Greenland picrites that are high like those from Hawaii owing to a comparable ΔT effect; however, this prediction is not consistent with measured Ni contents (Figure 8). One possibility is that Hawaii melted from a peridotite source that was unusually rich in nickel. However, this interpretation is not unique because the higher Ni contents of Hawaiian olivines, together with lower Ca and higher Fe/Mn, are also consistent with the expectations of pyroxenite melting (Sobolev et al. 2005; 2007; Herzberg 2011). Furthermore, both olivines and whole rock lava compositions in Mg-rich shield stage Hawaiian lavas are low in CaO; estimated high MgO primary melt compositions have lower CaO contents than experimental and thermodynamic melts of mantle peridotite (Walter, 1998; Herzberg 2006; Herzberg and Asimow 2008; Jennings and Holland 2015), consistent with pyroxenite melting.

COBALT CONTENTS OF OLIVINE AND MANTLE MELTS OF A PERIDOTITE SOURCE

Model Results

Compared with nickel, cobalt data for olivine are lacking in quality and quantity owing to its lower abundance levels. Also, there has never been a comparable understanding of how cobalt is partitioned between melts and olivine. Building on the success of the nickel modeling as discussed above, we will finish this contribution with a preliminary cobalt model.

Cobalt is more incompatible in olivine than Ni, but the partition coefficients depend on composition (equations 4 and 5). Cobalt contents of primary and derivative magmas and their crystallizing olivines have been calculated using the same procedure discussed above for nickel, using the partition coefficient from equation (5) (Beattie et al. 1991). These are compared with new high precision electron microprobe analyses of San Carlos olivine we provide in Table A6; our analytical method is discussed in the Appendix. We have found small differences in two San

Carlos olivine grain populations; one grain has an Mg number of 90.03 (±0.06; 1σ) and 139 (± 7; 1σ) ppm Co; another has an Mg number of 90.38 (0.04; 1σ) and 142 ppm (± 7; 1σ) Co. These data are similar to those reported by Sobolev et al. (2007; Mg number 90.22 and 140 ppm Co), and to 142 ppm Co reported by De Hoog et al. (2010) from LA-ICP-MS. Taken at face value, these data suggest a slight positive correlation of Mg number and Co content. Regression yields a model olivine at the solidus with an Mg number of 89.5 and 135 ppm Co, and we use this in our modeling. We assume peridotite KR4003 has a 105 ppm Co (McDonough and Sun 1995).

Primary magma solutions to the equation for accumulated fractional melting are shown in Figure 11a. Liquids extracted from dunite [L + Ol] and harzburgite [L + Ol + Opx] residues have similar Co contents at any specific MgO content. Co contents of liquids on the solidus can be higher by ~10 ppm for high MgO melts; Co contents of liquids extracted from lherzolite are an interpolation. The compositions of olivines in equilibrium with these primary magmas of accumulated fractional melting are shown in Figure 11b.

Olivine from Mantle Peridotite

Computed olivine compositions in equilibrium with primary magmas produced by accumulated fractional melting at mantle pressures are shown in Figure 12. These are in excellent agreement with those that have been measured for San Carlos olivine reported by Sobolev et al. (2007) and our new high precision electron microprobe data (Table A6). The computed olivine compositions are also in good agreement with olivine compositions from orogenic peridotite and xenoliths that have been measured by LA-ICP-MS (De Hoog et al. 2010). As with Ni, the agreement between observed and calculated olivine Co contents indicates a robust computational method constructed from Beattie-Jones, Toplis, and Herzberg-O'Hara parameterizations of experimental data.

Olivine from the Siqueiros Transform of the East Pacific Rise

High precision electron microprobe Co measurements made for olivines from the Siqueiros Transform are given in Table A4 and shown in Figure 13 together with those from the Knipovich ridge (Sobolev et al., 2007). Siqueiros olivine Co contents are in good agreement with those reported by Sobolev et al. (2007), and they are consistent with ~ 140 ppm Co calculated for olivines in equilibrium with primary magmas having 10-13% MgO. However, the olivine-only CLD at 1 atmosphere has generally lower Co than those which have been reported for olivines from the Knipovich MORB (Figure 13b; Sobolev et al. 2007). Similarly the calculated olivine-only LLD is lower in Co than those which have been measured for MORB glasses (Figure 13a; Jenner and O'Neill, 2012). We expect the elevated Co in both glasses and olivines are the result of plagioclase and clinopyroxene fractionation, but there are no partitioning data that permit a forward model and test of this conjecture.

Olivine from the Paleocene Picrites of West Greenland and Baffin Island (WGBI): The Ancient Icelandic Mantle Plume

New high precision Co analyses (Table A5) for olivines from West Greenland and Baffin Island lavas are compared with model olivines that crystallize from primary magmas (accumulated fractional melting) at 1 atmosphere. The primitive WGBI olivines with Mg numbers of 90.0 – 92.5 have Co contents that differ by about ± 10 ppm from the model olivines expected to crystallize from primary magmas (Figure 14). Olivines in some samples display coherent and clearly separable crystal line of descent trends, such as DUR3, DUR6 and PAD8, which are larger than the ± 7 ppm (1σ) uncertainty in the precision of our San Carlos olivines. In other samples, the scatter in Co is similar to the uncertainty in precision. Notably, the slightly higher Ni contents for West Greenland olivines compared with those from Baffin Island are not evident in Co.

Whole rock Co and MgO data reported by Larsen and Pedersen (2009) display a curved trend that coincides with a computed olivine-only LLD that extends from a primary magma having 20% MgO (Figure 14a). This MgO content is similar to the range of primary magma composition inferred from PRIMELT2 (Herzberg and Gazel 2009) and PRIMELT3 modeling (Hole and Millett 2016), which require a hot mantle plume source.

It is possible that the apparently well-resolved olivine Co contents for DUR3, DUR6 and PAD8 contain information about origin. In particular, an independent evaluation is needed of the model that WGBI lavas melted from a nickel-rich peridotite source by interaction with the core (Herzberg et al. 2013), as discussed above. This model predicts that the peridotite source might also be enriched in Co compared with the canonical 105 ppm because the partitioning of Co, like Ni, between silicate and sulfide liquids is pressure dependent (Siebert et al. 2012). However, this conclusion is based on a parameterization of experimental data up to 70 GPa, and it may not be extrapolated with confidence to 135 GPa at the core-mantle boundary. Furthermore, the effects of temperature, pressure, oxygen fugacity, and composition can add to significant uncertainties in the distribution coefficients for Ni and Co between silicate and metal liquid (Walter and Cottrell 2013). The main conclusion is that the rough agreement between observed and calculated olivine Co is supportive of the Beattie-Jones, Toplis, and Herzberg-O'Hara parameterizations to within ± 20 ppm (1σ).

IMPLICATIONS

Forward models of partial melting and crystallization of a peridotite source using existing olivine-liquid partitioning for Ni, Co, Fe, Mn, and Mg (Beattie et al. 1991;Toplis 2005; Herzberg and O'Hara 2002; Matzen et al. 2013) constrain the origins of measured olivines from mantle peridotite and a wide range of related igneous rocks. Cobalt contents of olivine are significantly lower than are Ni contents, and there are fewer high precision Co data. Implications about origin are based mostly on high precision electron microprobe analysis of Ni, Fe, Mn, and Mg, and there is generally good agreement where high precision Co data are available.

Olivines in mantle peridotite have Ni contents and Mg numbers that were largely determined by an initial stage of equilibrium crystallization in a turbulently convecting early Earth magma ocean; subsequent stages of partial melting operated to slightly elevate Ni and Mg number in peridotite residues and its olivines.

Olivines from Archean komatiites from the Abitibi greenstone belt have Ni contents and Mg numbers that are consistent with extensive melting peridotite source at great depths in the mantle. This olivine chemistry is also consistent with primary magmas that contained 30% MgO.

Some olivines from mid-ocean ridge basalts have Ni and Co contents and Mg numbers that are similar to those of model olivines from primary magmas having ~ 11.5% MgO; however, most have compositions that can be attributed to magma chamber crystallization, recharge, and mixing (Coogan and O'Hara 2002; O'Hara and Herzberg 2002; O'Neill and Jenner), in addition to sequestration from a sulfide phase (Herzberg 2011).

Olivines from the present-day Icelandic mantle plume have compositions that are consistent with magma chamber crystallization, recharge, and mixing imposed on a primary magma having about 17.6% MgO that formed by melting a peridotite source; unlike Hawaii, the melting of recycled crust as a distinct pyroxenite lithology is not evident in olivine chemistry of Iceland.

Paleocene picrites from Baffin Island and West Greenland from the ancient Icelandic plume have olivines with Ni contents that are consistent with either Ni-rich peridotite that formed by core-mantle interaction (Herzberg et al. 2013) or by low pressure crystallization of hot and deep magmas (Matzen et al. 2013).

Olivine faithfully records in its chemistry the widespread occurrence of magma chamber fractional crystallization, recharge, and mixing (O'Hara 1977). These processes typically elevate the Ni content of olivine, and can potentially compromise interpretations of source lithology.

In summary, the partitioning of Ni, Mg and Fe between olivine and liquid provides a successful foundation for understanding the compositions of naturally-occurring olivine that formed in an extremely wide range of temperature and pressure conditions on Earth. In general, hot magma oceans, mantle plumes, and ambient mantle magmatism form in ways that are captured by the compositions of the olivine crystals that they contained.

ACKNOWLEDGMENTS

We are honored and grateful to Keith Putirka for his kind invitation to contribute this paper to the Centennial Issue of the American Mineralogist, and for a thoughtful review. Mike Garcia is thanked for editorial handling. Fin Stuart is thanked for collecting the Baffin Island samples from which thin sections were made, and Lotte Larsen is thanked for comments. Michael Perfit is

thanked for providing samples from the Siqueiros fracture zone, and Michael Baker is thanked for comments. We are most grateful to Andrew Matzen and Chusi Li for critical reviews.

REFERENCES CITED

Ahern, J.L., and Turcotte, D. (1979) Magma migration beneath an ocean ridge. Earth and Planetary Science Letters, 46,115-122.

Arndt, N.T., Lesher, C.M., and Barnes, S.J. (2008) *Komatiite*. Cambridge University Press, Cambridge, 467 pp.

Barnes, S.J., Godel, B., Gürer, D., Brenan, J.M., Robertson, J., and Paterson, D. (2013) Sulfide-olivine Fe-Ni exchange and the origin of anomalously Ni rich magmatic sulfides. Economic Geology, 108, 1971-1982.

Beattie, P., Ford, C., and Russell, D. (1991) Partition coefficients for olivine-melt and orthopyroxene-melt systems. Contributions to Mineralogy and Petrology, 109, 212-224.

Burke, K., Steinberger, B., Torsvik, T.H., and Smethurst, M.A. (2008) Plume generation zones at the margines of Large Low Shear Velocity Provinces on the core-mantle boundary. Earth and Planetary Science Letters, 265, 49-60.

Carlson, R.W., Garnero, E., Harrison, T.M., Li, J., Manga, M., McDonough, W.F., Mukhopadhyay, S., Romanowicz, B., Rubie, D., Williams, Q., and Zhong, S. (2014) How did early Earth become our modern world? Annual Review of Earth and Planetary Sciences, 42, 151-178.

Caro, G., Bourdon, B., Wood, B.J., Corgne, A. (2005) Trace-element fractionation in Hadean mantle generated by melt segregation from a magma ocean. Nature, 436, 246–249.
Coogan, L.A., and O'Hara, M.J. (2015) MORB differentiation: *In situ* crystallization in replenished-tapped magma chambers. Geochimical et Cosmochimica Acta, 158, 147-161.

Coltice, N., Moreira, M., Hernlund, J., and Labrosse, S. (2011) Crystallization of a basal magma ocean recorded by Helium and Neon. Earth and Planetary Science Letters, 308, 193-199.

Corgne, A., Liebske, C., Wood, B.J., Rubie, D.C., and Frost, D.J. (2005) Silicate perovskite-melt partitioning of trace elements and geochemical signature of a deep perovskite reservoir. Geochimica et Cosmochimica Acta, 69, 485-496.

Darbyshire, F.A., White, R.S., and Priestley, K.F. (2000) Structure of the crust and uppermost mantle of Iceland from a combined seismic and gravity study. Earth and Planetary Science Letters 181, 409-428.

De Hoog, J.C.M., Gall, L., and Cornell, D.H. (2010) Trace-element geochemistry of mantle olivine and application to mantle petrogenesis and geothermobarometry. Chemical Geology, 270, 196-215.

Doucet, L.S., D.A., Ionov, A.V. Golovin, and N.P. Pokhilenko (2012) Depth, degrees and tectonic settings of mantle melting during craton formation: inferences from major and trace element compositions of spinel harzburgite xenoliths from the Udachnaya kimberlite, central Siberia. Earth and Planetary Science Letters, 359-360, 206-218.

Elkins-Tanton, L.T. (2008) Linked magma ocean solidification and atmospheric growth for Earth and Mars. Earth and Planetary Science Letters, 271, 181-191.

Farnetani, C.G., and Hofmann, A.W. (2009) Dynamics and internal structure of a lower mantle plume conduit. Earth and Planetary Science Letters, 282, 314-322.

Filiberto, J., Jackson, C., Le, L., and Treiman, A.H. (2009) Partitioning of Ni between olivine and an iron-rich basalt: experiments, partition models, and planetary implications. American Mineralogist, 94, 256-261.

Fitton, J.G., Saunders, A.W., Kempton, P.D., and Hardarson, B.S. (2003) Does depleted mantle form an intrinsic part of the Icelandic plume? Geochemistry, Geophysics, Geosystems 4, 1032, doi:10.1029/2002GC000424.

Hamano, K., Abe, Y. and Genda, H. (2013) Emergence of two types of terrestrial planet on solidification of magma ocean. Nature, 497, 607-610.

Hart S.R., and Davis ,K.E .(1978) Nickel partitioning between olivine and silicate melt. Earth and Planetary Science Letters, 40, 203–219.

Herd, C.D.K., Dwarzki, R.E.D., and Shearer, C.K. (2009) The behavior of Co and Ni in olivine in planetary basalts: an experimental investigation. American Mineralogit, 94, 244-255.

Herzberg, C. (2004) Geodynamic information in peridotite petrology. Journal of Petrology, 45, 2507-2530.

Herzberg, C. (2006) Petrology and thermal structure of the Hawaiian plume from Mauna Kea volcano. Nature, 444, 605-609.

Herzberg, C. (2011) Identification of Source Lithology in the Hawaiian and Canary Islands: Implications for Origins. Journal of Petrology, 52, 113-146.

Herzberg, C. (2015) Petrological evidence from komatiites for an early Earth carbon and water cycle. Journal of Petrology, submitted.

Herzberg, C.T., and O'Hara, M.J. (1985) Origin of mantle peridotite and komatiite by partial melting. Geophysical Research Letters, 12, 541-544.

Herzberg, C., and Zhang, J. (1996) Melting experiments on anhydrous peridotite KLB-1: Compositions of magmas in the upper mantle and transition zone. Journal of Geophysical Research, 101, 8271-8295.

Herzberg, C., and Asimow P.D. (2008) Petrology of some oceanic island basalts: PRIMELT2.XLS software for primary magma calculation, Geochemistry, Geophysics, Geosystems 8, doi:10.1029GC002057.

Herzberg, C., and O'Hara, M.J. (2002) Plume-associated ultramafic magmas of phanerozoic age. Journal of Petrology, 43, 1857-1883.

Herzberg, C., and E. Gazel (2009) Petrological evidence for secular cooling in mantle plumes. Nature, 458, 619-622.

Herzberg, C., and Asimow, P.D. (2015) PRIMELT3 MEGA.XLSM software for Primary Magma Calculation: Peridotite Primary Magma MgO Contents from the Liquidus to the Solidus. Geochemistry, Geophysics, Geosystems**,** 16, 563-578, doi:10.1002/2014G005631.

Herzberg, C., Condie, K., and Korenaga, J. (2010) Thermal history of the Earth and its petrological expression. Earth and Planetary Science Letters, 292, 79-88.

Herzberg, C., Asimow, P., Ionov, D., Vidito, C., Jackson, M.G., and Geist, D. (2013) Nickel and helium evidence for melt above the core-mante boundary. Nature, 493, 393-397.

Herzberg, C., Cabral, R.A., Jackson, M.D., Vidito, C., Day, J.M.D., and Hauri, E. (2014) Phantom Archean crust in Mangaia hotspot lavas and the meaning of heterogeneous mantle. Earth and Planetary Science Letters, 396, 97-106.

Hole, M.J., and Millett, J.M. (2016) Controls of mantle potential temperature and lithospheric thickness on magmatism in the North Atlantic Igneous Province. Journal of Petrology, in press.

Ionov, D.A. (2007) Compositional variations and heterogeneity in fertile lithospheric mantle: peridotite xenoliths in basalts from Tariat, Mongolia. Contributions to Mineralogy and Petrology, 154, 455–477.

Ionov, D.A. (2010) Petrology of mantle wedge lithosphere: New data on supra-subduction zone peridotite xenoliths from the andesitic Avacha volcano, Kamchatka. Journal of Petrology, 51**,** 327-361.

Ionov, D.A., and Hofmann, A.W. (2007) Depth of formation of subcontinental off-craton peridotites. Earth and Planetary Science Letters, 261, 620-634.

Ionov, D.A., Ashchepkov, I., and Jagoutz, E. (2005) The provenance of fertile off-craton lithospheric mantle: Sr-Nd isotope and chemical composition of garnet and spinel peridotite xenoliths from Vitim, Siberia. Chemical Geology, 217, 41-74.

Ito, G., and Mahoney, J.J. (2005) Flow and melting of a heterogeneous mantle: 1. Method and importance to the geochemistry of ocean island and mid-ocean ridge basalts. Earth and Planetary Science Letters, 230, 29–46.

Jackson, M.G., Carlson, R.W., Kurz, M.D., Kempton, P.D., Francis, D., and Blusztajn, J. (2010). Evidence for the survival of the oldest terrestrial mantle reservoir. Nature, 466, 853-856.

Jenner, F.E., and O'Neill, H. St.C. (2012) Analysis of 60 elements in 616 ocean floor basaltic glasses. Geochemistry, Geophysics, Geosystems, 13, Q02005, doi:10.1029/2011GC004009.

Jennings, E.S., and Holland, T.J.B. (2015) A simple thermodynamic model for melting of peridotite in the system NCFMASOCr. Journal of Petrology, 56, 869-892.

Jones, J.H. (1984) Temperature and pressure- independent correlations of olivine-liquid partition coefficients and their application to trace element partitioning. Contributions to Mineralogy and Petrology, 88, 126-132.

Labrosse, S., Hernlund, J.W., and Coltice, N. (2007) A crystallizing dense magma ocean at the base of the Earth's mantle. Nature, 450, 866-869.

Larsen, L.M., and Pedersen, A.K. (2000) Processes in high-Mg, high-T magmas: evidence from olivine, chromite and glass in Palaeogene picrites from West Greenland. Journal of Petrology, 41, 1071-1098.

Larsen, L.M., and Pedersen, A.K. (2009) Petrology of the Paleocene picrites and flood basalts on Disko and Nuussuaq, West Greenland. Journal of Petrology, 50, 1667-1711.

Lee, C.-T., Leeman, W.P., Canil, D., and Li, Z.-X.,A. (2005). Similar V/Sc systematic in MORB and arc basalts: implications for oxygen fugacities of their mantle sources. Journal of Petrology, 46, 2313-2336.

Lesher, C.E., and Walker, D. (1988) Cumulate maturation and melt migration in a temperature gradient. Journal of Geophysical Research, 93, 10295-10311.

Li, C., and Ripley, E.M. (2010) The relative effects of composition and temperature on olivine-liquid Ni partitioning: Statistical deconvolution and implications for petrologic modeling. Chemical Geology, 275, 99-104.

Li, J., and Agee, C.B. (2001) The effect of pressure, temperature, oxygen fugacity and composition on partitioning of nickel and cobalt between liquid Fe-Ni-S alloy and liquid silicate: implications for the earth's core formation. Geochimica et Cosmochimica Acta, 65, 1821-1832.

Li, X., Kind, R., Priestley, K., Sobolev, S.V., Tilmann, F., Yuan, X. & Weber, M. (2000) Mapping the Hawaiian plume conduit with converted seismic waves. Nature, 405, 938-941.

Li, X. Kind, R. Yuan, X., Wölbern, I. & Hanka, W. (2004) Rejuvenation of the lithosphere by the Hawaiian plume. Nature, 427, 827-829.

Lightfoot, P. C., Hawkesworth, C. J., Olshevsky, K., Green, A., Doherty,W., and Keays, R. R. (1997) Geochemistry of Tertiary tholeiites and picrites from Qeqertarssuaq (Disko Island) and Nuussuaq,West Greenland with implications for the mineral potential of comagmatic intrusions. Contributions to Mineralogy and Petrology, 128, 139-163.

Longhi, J., Durand, S.R., and Walker, D. (2010) The pattern of Ni and Co abundances in lunar olivines. Geochimica et Cosmochimica Acta, 74, 784-798.

Lupu, R.E., Zahnle, K., Marley, M.S., Schaefer, L., Fegley, B., Morley, C., Cahoy, K., Freedam, R., and Fortney, J.J. (2014) The atmospheres of Earthlike planets after giant impact events. The Astrophysics Journal, 784, 27. (doi:10.1088/0004-637X/784/1/27).

Mallmann, G., and O'Neill, H.St.C. (2009) The crystal/melt partitioning of V during mantle melting as a function of oxygen fugacity compared with some other elements (Al, P, Ca, Sc, Ti, Cr, Fe, Ga, Y, Zr, and Nb). Journal of Petrology, 50, 1765-1794.

Matzen, A.K., Baker, M.B., Beckett, J.R., and Stolper, E.M. (2011) Fe-Mg partitioning between olivine and high-magnesium melts and the nature of Hawaiian parental magmas. Journal of Petrology, 52, 1243-1263.

Matzen, A.K., Baker, M.B., Beckett, J.R., and Stolper, E.M. (2013) The temperature and pressure dependence of nickel partitioning between olivine and silicate melt. Journal of Petrology, 54, 2521-2545.

Matzen, A.K., Baker, M.B., Beckett, J.R., Wood, B.J., and Stolper, E.M. (2016) The effect of liquid composition on the partitioning of Ni between olivine and silicate melt. Contributions to Mineralogy and Petrology, submitted.

McNamara, A.K., Garnero, E.J., and Rost, S. (2010) Tracking deep mantle reservoirs with ultra-low velocity zones. Earth and Planetary Science Letters, 299, 1-9.

McKenzie, D. (1984) The generation and compaction of partial melts. Journal of Petrology, 25, 713-765.

McDonough, W.F., and Sun, S.-s. (1995) The composition of the Earth. Chemical Geology, 120, 223-253.

Melosh, H. J. (1990). Giant impacts and the thermal state of the early Earth. In Origin of the Earth (Edited by J. H. Jones and H. E. Newsom) pp. 69-84, Oxford University Press, New York.

Morgan, J.P. (2001) Thermodynamics of pressure release melting of a veined plum pudding mantle. Geochemistry, Geophysics, Geosystems, 2, 2000GC000049.

Mulyukova, E., Steinberger, B., Dabrowski, M., and Sobolev, S.V. (2015) Survival of LLSVPs for billions of years in a vigorously convecting mantle: replenishment and destruction of chemical anomaly. Journal of Geophysical Research, Solid Earth, 120, doi:10.1002/2014JB011688.

Mysen, B.O. (2006) Redox equilibria and melt structure: implications for olivine/melt element partitioning. Geochimica et Cosmochimica Acta, 70, 3121-3138.

Mysen, B.O. (2007) Partitioning of calcium, magnesium, and transition metals between olivine and melt governed by the structure of the silicate melt at ambient pressure. American Mineralogist, 92, 844-862.

Niu, Y., Wilson, M., Humphreys, E.R., and O'Hara, M.J. (2011) The origin of intra-plate ocean island basalts (OI B): the lid effect and its geodynamic implications. Journal of Petrology, 52, 1443-1468.

O'Hara, M.J. (1968) The bearing of phase equilibria studies in synthetic and natural systems on the origin of basic and ultrabasic rocks. Earth Science Reviews, 4, 69-133.

O'Hara, M. J. (1977) Geochemical evolution during fractional crystallization of a periodically refilled magma chamber. Nature, 266, 503–507.

O'Hara M. J., and Herzberg C. (2002) Interpretation of trace element and isotope features of basalts: relevance of field relations, petrology, major element data, phase equilibria, and magma chamber modeling in basalt petrogenesis. Geochimica et Cosmochimica Acta, 66, 2167–2191.

O'Neill, H.St.C and Jenner, F.E. (2012) The global patter of trace-element distributions in ocean floor basalts. Nature 491, 698-704.

Rizo, H., Boyet, M., Blichert-Toft, J., and Rosing, M. (2011) Combined Nd and Hf isotope evidence for deep-seated source of Isua lavas. Earth and Planetary Science Letters, 312, 267–279.

Roeder P.L., and Emslie, R.F. (1970) Olivine-liquid equilibrium. Contributions to Mineralogy and Petrology, 29, 275-289.

Pertermann, M., and Hirschmann, M.M. (2003) Anhydrous partial melting experiments on MORB-like eclogite: phase relations, phase compositions and mineral-melt partitioning of major elements at 2–3 GPa. Journal of Petrology, 44, 2173–2201.

Puchtel, I.S., Blichert-Toft, J., Touboul, M., Walkter, R.J., Byerly, G.R., Nisbet, E.G., and Anhauser, C.R. (2013). Insights in early Earth from Barberton komatiites: evidence from lithophile isotope and trace element systematic. Geochimica et Cosmochimica Acta, 108, 63-90.

Putirka, K. (2016) Cooling rates for Earth, Moon, Mars and Vesta, and new models for oxygen fugacity, ferric-ferrous ratios, olivine-liquid Fe-Mg exchange, and mantle potential temperatures. American Mineralogist, in press.

Putirka, K., Ryerson, F.J., Perfit, M., and Ridley, W.I. (2011) Mineralogy and composition of the oceanic mantle. Journal of Petrology, 52, 279-313.

Rubie, D., Frost, D.J., Mann, U., Asahara, Y., Nimmo, F., Tsuno, K., Kegler, P., and Palme, H. (2011) Heterogeneous accretion, composition, and core-mantle differentiation of the Earth. Earth and Planetary Science Letters, 301, 31-42 (2011).

Saunders, A.D., Fitton, J.G., Kerr, A.C., Norry, M.J., and Kent, R.W. (1997) The North Atlantic Igneous Province (edited by J.J. Mahoney and M.J. Coffin) Geophysical Monograph Series,100, pp. 45-93, AGU, Washington DC.

Shorttle, O., Maclennan, J. (2011) Compositional trends of Icelandic basalts: implications for short-length scale lithological heterogeneity in mantle plumes. Geochemistry, Geophysics, Geosystems,12, Q11008. http://dx.doi.org/10.1029/2011GC003748.

Shorttle, O., Maclennan, J., and Lambart, S. (2014) Quantifying lithological variability in the mantle. Earth and Planetary Science Letters, 195, 24-40.

Siebert, J., Badro, J., Antonangeli, D., and Ryerson, F.J. (2012) Metal-silicate partitioning of Ni and Co in a deep magma ocean. Earth and Planetary Science Letters, 321, 189-197.

Sobolev, A.V., Hofmann, A.W., Sobolev, S.V., and Nikogosian I.K. (2005) An olivine-free mantle source of Hawaiian shield basalts. Nature, 434, 590-597.

Sobolev, A.V., Hofmann, A.W., Kuzmin, D.V., Yaxley, G.M., Arndt, N.T., Chung, S.-L., Danyushevsky, L.V., Elliott, T., Frey, F.A., Garcia, M.O., Gurenko, A.A., Kamenetsky, V.S., Kerr, A.C., Krivolutskaya, N.A., Matvienkov, V.V., Nikogosian, I.K., Rocholl, A., Sigurdsson, I.A., Sushchevskaya, N.M., and Teklay M. (2007) The amount of recycled crust in sources of mantle-derived melts. Science, 316, 412-417.

Sobolev, A.V., Asafov, E.V., Gurenko, A.A., Arndt, N.T., Batanova, V.G., Portnyagin, M.V., Garbe-Schönberg, D., and Krasheninnikov, S.P. (2016) Komatiites reveal a hydrous Archaean deep-mantle reservoir. Nature, 531, 628-632.

Solomatov, V. (2015) Magma oceans and primordial mantle differentiation. In Treatise on Geophysics, (Shubert, G. Ed.), 2nd edition, 9, 81-104.

Starkey, N.A., Stuart, F.M., Ellam, R.M., Fitton, J.G., Basu, S., and Larsen, L.M. (2009) Helium isotopes in early Iceland plume picrites: Constraints on the composition of high $^{3}He/^{4}He$ mantle. Earth and Planetary Science Letters, 277, 91-100.

Straub, S. M., LaGatta, A. B., Martin-Del Pozzo, A. L. and Langmuir, C. H. (2008) Evidence from high Ni olivines for a hybridized peridotite/pyroxenite source for orogenic andesites from the central Mexican Volcanic Belt. Geochemistry, Geophysics, Geosystems, 9, Q03007, doi:10.1029/2007GC001583.

Stuart, F.M., Lass-Evans, S., Fitton, J.G., and Ellam, R.M. (2003) High $^{3}He/^{4}He$ ratios in picritic basalts from Baffin Island and the role of a mixed reservoir in mantle plumes. Nature, 424, 57-59.

Takahashi, E. (1978) Partitioning of Ni^{2+}, Co^{2+}, Fe^{2+} , Mn^{2+} , and Mg^{2+} between olivine and silicate melts: compositional dependence of partition coefficient. Geochimica et Cosmochimica Acta, 42, 1829-1844.

Tonks, W.B., and H. J. Melosh, H.J. (1990) The physics of crystal settling and suspension in a turbulent magma ocean. In Origin of the Earth (edited by J. H. Jones and H. E. Newsom), 151-174, Oxford University Press, New York.

Tonks, W.B., and Melosh, H.J. (1993) Magma ocean formation due to giant impacts. Journal of Geophysical Research, 98, 5319–5333.

Trela, J., Vidito, C., Gazel, E., Herzberg, C., Class, C., Whalen, W., Jicha, B., Bizimis, M., and Alvarado, G.E. (2015) Recycled crust in the Galápagos plume source at 70 Ma: implications for plume evolution. Earth and Planetary Science Letters 425, 268-277.

Walker, D. (2005) Core-mantle chemical issues. Canadian Mineralogist, 43, 553-1564.

Walter, M.J. (1998) Melting of garnet peridotite and the origin of komatiite and depleted lithosphere. Journal of Petrology, 39, 29-60.

Walter, M.J., and Trønnes, R.G. (2004) Early Earth differentiation. Earth and Planetary Science Letters, 225, 253-269.

Walter, M.J., and Cottrell, E. (2013) Assessing uncertainty in geochemical models for core formation in Earth. Earth and Planetary Science Letters, 365, 165-176.

Wang, Z., and Gaetani, G.A. (2008) Partitioning of Ni between olivine and siliceous eclogite partial melt: experimental constraints on the mantle source of Hawaiian basalts. Contributions to Mineralogy and Petrology, 156, 661-678.

Weis, D., Garcia, M.O., Rhodes, J.M., Jellinek, M., and Scoates, J.S. (2011) Role of deep mantle in generating the compositional asymmetry of the Hawaiian mantle plume. Nature Geoscience, 4, 831-838.

Yaxley, G.M., and Green, D.H. (1998). Reactions between eclogite and peridotite: mantle refertilisation by subduction of oceanic crust. Schweiz. Mineral. Petrogr. Mitt., 78, 243–255.

Zhang, J., and Herzberg, C.T. (1994) Melting experiments on anhydrous peridotite KLB-1 from 5.0 to 22.5 GPa. Journal of Geophysical Research, 99, 17,729-17,742.

FIGURE 1. Experimentally measured $D_{NiO}^{Ol/L}$ and its model prediction (Beattie et al., 1991; Matzen et al., 2013), where $D_{NiO}^{Ol/L}$ is expressed on a weight% basis (i.e., wt% NiO in olivine/wt% NiO in melt). For Beattie et al. (1991), weight % D = mole% × 1.135. For Matzen et al. (2013), weight % D = mole% × 0.5318. The database consists of 284 individual experimental olivine-melt pairs, and is given in Table A2 of the Appendix.

FIGURE 2. Model nickel contents of peridotite-source primary magmas and their equilibrium olivines. Primary magma compositions are solutions to the equations for batch and accumulated fractional melting (i.e., AFM) using an initial source composition having 0.25% NiO (i.e., 1964 ppm Ni). Equilibrium olivine compositions at pressures of melt generation are computed from Beattie-Jones, Toplis, and Herzberg-O'Hara parameterizations. Please see text for details. a) Blue lines are tie lines connecting olivine composition to liquids in equilibrium with olivine only (i.e., L+Ol). Red line labeled solidus are Ni and MgO contents of melts on the solidus; black space between red and green lines are Ni contents of primary melts for the assemblages (L+Ol±Opx±Cpx±Sp±Gr). b) Effects of peridotite composition and melting mechanism on the Ni and MgO contents of melts. Green squares are off-craton peridotite xenolith data from Asia (Ionov 2007; 2010; Ionov and Hofmann 2007; Ionov et al. 2005).

FIGURE 3. Nickel contents and Mg numbers (i.e., mole% 100MgO/(MgO + FeO)) for model and measured olivines. a) black and red forms are olivine compositions in equilibrium with batch and accumulated fractional melts, respectively, using the Beattie-Jones parameterization. Gray shaded form with ± 1σ represents the 1 *Absolute* RMSE uncertainty in olivine Ni content that is propagated from uncertainties in experimental data (Table A2 and Herzberg et al. 2013). Black cross is olivine composition at the liquidus for near-total melting. Mg number is mole% 100MgO/(MgO + FeO). Blue form bounds olivine compositions calculated by Straub et al. (2008); Mg numbers for olivines appropriate for near-solidus and near-liquid melts are ~ 89.5 and 96.0. b) comparison of model olivines of batch primary magmas with experimentally-measured olivines (Herzberg and Zhang 1996; Table A3); MgO and FeO contents of olivines distributed between the liquidus and solidus were illustrated in Figures 4, 5, and 6 in Herzberg and Zhang (1996).

FIGURE 4. Nickel contents and Mg numbers (i.e., mole% 100MgO/(MgO + FeO)) for model olivines compared with 215 measured olivines in mantle peridotite (Herzberg et al. 2013). a) model olivines in equilibrium with accumulated fractional melts in the mantle. b) model olivines in equilibrium with batch melts in the mantle.

FIGURE 5. Nickel contents and Mg numbers (i.e., mole% 100MgO/(MgO + FeO)) of model olivines compared with measured olivines from Archean komatiites and Makapuu-stage Koolau volcano, Hawaii (Sobolev et al. 2007). Melting is assumed to be accumulated fractional (Herzberg 2004), and olivine crystallizes from primary magmas at the surface; this is more clearly shown and described in Figure 6. Green lines are model CLD for primary magmas having the MgO contents in the 20 to 30% range; note the model olivine CLD is concaved toward the Mg number axis, in good agreement with measured olivines.

FIGURE 6. Nickel contents and Mg numbers (i.e., mole% 100MgO/(MgO + FeO)) of model and measured olivines. Model olivine compositions for a Siqueiros MORB primary magma is given in Herzberg and Asimow (2015; MgO = 11.56%), and is likely representative of all MORB. Open cross is olivine in equilibrium with the primary magma having a Ni content as described by equation (10). Olivine crystal line of descent CLD is compared with measured olivines from the Siqueiros fracture zone (Table A4) and South East Indian Ridge (Sobolev et al. 2007). The CLD calculation was made with PRIMELT3 (Herzberg and Asimow 2015) for fracationation of olivine, and MELTS (Ghioro and Sack 1995) for fractionation of olivine + plagioclase and olivine + plagioclase + clinopyroxene at 200 bars, an oxygen fugacity defined by the QFM buffer and with 0.2% H_2O. Olivine compositions were computed using Fe-Mg partitioning from Toplis (1995). Ni partition coefficients used: olivine-melt from Beattie et al. (1991); plagioclase-melt = 0; clinopyroxene-melt = 0.25 $D_{NiO}^{Ol/L}$ (Herzberg et al. 2013). It is notable that MELTS is not sufficiently calibrated for Ni, and also underestimates olivine Mg number by ~ 2%; we use the MELTS CLD and compute olivine Mg number from Toplis (1995). Note also that model olivines at high pressure have slightly lower Mg numbers than those at the surface, and this is accommodated by higher K_D in the models of Herzberg and O'Hara (2002) and Toplis (2005). Therefore, olivines that crystallize from a primary magma at the surface (black form) will have higher Mg numbers than residual olivines at mantle depths (red form), and their range of compositions is highly restricted.

FIGURE 7. Nickel contents and Mg numbers (i.e., mole% 100MgO/(MgO + FeO)) of model olivines compared with measured olivines from Theistareykir volcano, Iceland and Makapuu-stage Koolau volcano, Hawaii (Sobolev et al. 2007). All model olivines are assumed to crystallize at 1 atmosphere. Open cross is the composition of olivine that would crystallize from the primary magma containing 17.6% MgO and Ni as given by equation (10); this is a PRIMELT3 primary magma solution (Herzberg and Asimow 2015) for Theistareyker lava sample TH03xrf (Shorttle et al. 2014). Black lines labeled L+Ol, L+Ol+Plag, and L+Ol+Plag+Cpx describe the compositions of olivine that would crystallize along the liquid line of descent (i.e., CLD) at 1 atmosphere, anhydrous and at an oxygen fugacity defined by the QFM buffer. Arrow labeled P describes the effect of pressure on the L+Ol+Plag+Cpx CLD. The CLD calculation was made with PRIMELT3 (Herzberg and Asimow 2015) and MELTS (Ghioro and Sack 1995) as described in Figure 6b for MORB, but for 0% H_2O. Red lines are compositions of olivines that would crystallize from magmas that form by mixing of the primary magma with derivative magmas along the LLD. White circles are Ni contents of olivine calculated using the method of Matzen et al. (2013; their experiments combined with a compilation of literature data; 2975 ppm Ni in olivine in residual peridotite). In all cases olivine is assumed to crystallize near the surface. White circles are for the following 5 conditions of melt segregation in the mantle, from lowest to highest Ni contents: 1) 0 GPa & 1399°C, 2) 0.5 GPa 1426°C, 3) 1 GPa & 1451°C, 4) 1.5 GPa & 1476°C, 5) 1504°C & P = 2.1 GPa (Hole and Millet 2016). In all cases, these temperatures T at pressures P are calculated from equations 12 and 13 in Herzberg & Asimow (2015). Melting pressures refer to final melting of the mantle region, not pressures at which melting initiates.

FIGURE 8. Nickel contents and Mg numbers (i.e., mole% 100MgO/(MgO + FeO)) of model olivines compared with measured olivines from West Greenland and Baffin Island (Table A5).

Model olivines are those that crystallize from primary magmas at the surface; melting mechanism is accumulated fractional melting. Olivines that crystallize from primary magmas have been calculated using the Beattie-Jones model and peridotite sources having 1964 (McDonough and Sun 1995) and 2360 ppm Ni. Crystal line of descent and mixing lines are from Figure 7. White circles are calculated Ni contents of olivine using the method of Matzen et al. (2013; their experiments combined with a compilation of literature data; 2975 ppm Ni in olivine in residual peridotite; primary magma MgO = 20.0%) for the following conditions: high Ni using melting T = 1580°C & P = 2.8 GPa (Herzberg and Asimow 2015; Hole and Millet 2016) and crystallization T = 1444°C & 1 atmosphere (Herzberg & Asimow 2015); low Ni using melting T = 1549°C & P = 2.1 GPa and crystallization T = 1444°C & 1 atmosphere (Herzberg & Asimow 2015; Hole and Millet 2016). Melting pressures refer to final melting of the mantle region, not pressures at which melting initiates.

.

FIGURE 9. Fe/Mn and Mg numbers of model olivines compared with measured olivines. Data from the South East India Rise, Theistareykir, Hawaii are from Sobolev et al. (2007); data from West Greenland and Baffin Island are from this work (Table A5). Black form is model olivines of a peridotite source having 0.13% MnO (Herzberg 2011). Measured olivines from Iceland are consistent with model olivines of a peridotite source having Mg numbers > 90 and Fe/Mn in the 62 to 66 range. Fractional crystallization of olivine does not change Fe/Mn very much, but clinopyroxene fractionation can elevate Fe/Mn (Herzberg et al. 2014; Trela et al. 2015). Olivines from Hawaii have Fe/Mn that are higher than those expected of peridotite-source melting, owing possibly to retention of Mn in a garnet pyroxenite source, and elevation of primary melt Fe/Mn from which the olivines crystallized (Herzberg 2011).

FIGURE 10. Histograms of V/Sc for West Greenland and Baffin Island lavas that have been filtered with Nd and Sr isotope ratios to exclude samples that have experienced crustal contamination. West Greenland lavas generally have higher V/Sc, consistent with deeper melting of garnet peridotite.

FIGURE 11. Model cobalt contents of peridotite-source primary magmas and their equilibrium olivines. Primary magma compositions are solutions to the equations for batch and accumulated fractional melting (i.e., AFM) using an initial source composition having 105 ppm Co (McDonough and Sun 1995). Equilibrium olivine compositions at pressures of melt generation and 1 atmosphere are computed from Beattie-Jones, Toplis, and Herzberg-O'Hara parameterizations (please see text for details). Gray shaded form in panel b) is the 1 σ uncertainty in olivine composition for AFM partial melts arising from application of the Beattie et al. (1991) parameterization (i.e., equation 5) to experimental data (Herd et al. 2009; Longhi et al. 2010; Mysen 2006; 2007; Takahashi 1978).

FIGURE 12. Cobalt contents and Mg numbers (i.e., mole% 100MgO/(MgO + FeO)) of model and measured olivines from mantle peridotite. Model olivines are those in equilibrium with primary magmas of accumulated fractional melting. Measured olivines are those for San Carlos olivine (Table A6; Sobolev et al. 2007), and olivines in peridotite from orogenic and xenoliths occurrences (De Hoog et al. 2010).

FIGURE 13. Model cobalt contents of peridotite-source primary magmas, their equilibrium olivines compared with observed cobalt contents of MORB glasses and olivines. Model results are from Figure 11. a) Measured MORB glasses are from Jenner and O'Neill (2012). b) Measured olivines are from the Siqueiros transform of the East Pacific Rise (Table A4 and Sobolev et al. 2007) and Knipovich ridge (Sobolev et al., 2007).

FIGURE 14. Model cobalt contents of peridotite-source primary magmas, their equilibrium olivines compared with observed cobalt contents of whole rocks and olivines from West Greenland and Baffin Island. Model results are from Figure 11. a) Measured whole rocks are from Larsen and Pedersen (2009; red symbols). b) Measured olivines are from Baffin Island (i.e., BI sample numbers) and West Greenland (i.e., WG sample numbers) (Table A5).

This is a preprint, the final version is subject to change, of the American Mineralogist (MSA)
Cite as Authors (Year) Title. American Mineralogist, in press.
(DOI will not work until issue is live.) DOI: http://dx.doi.org/10.2138/am-2016-5538

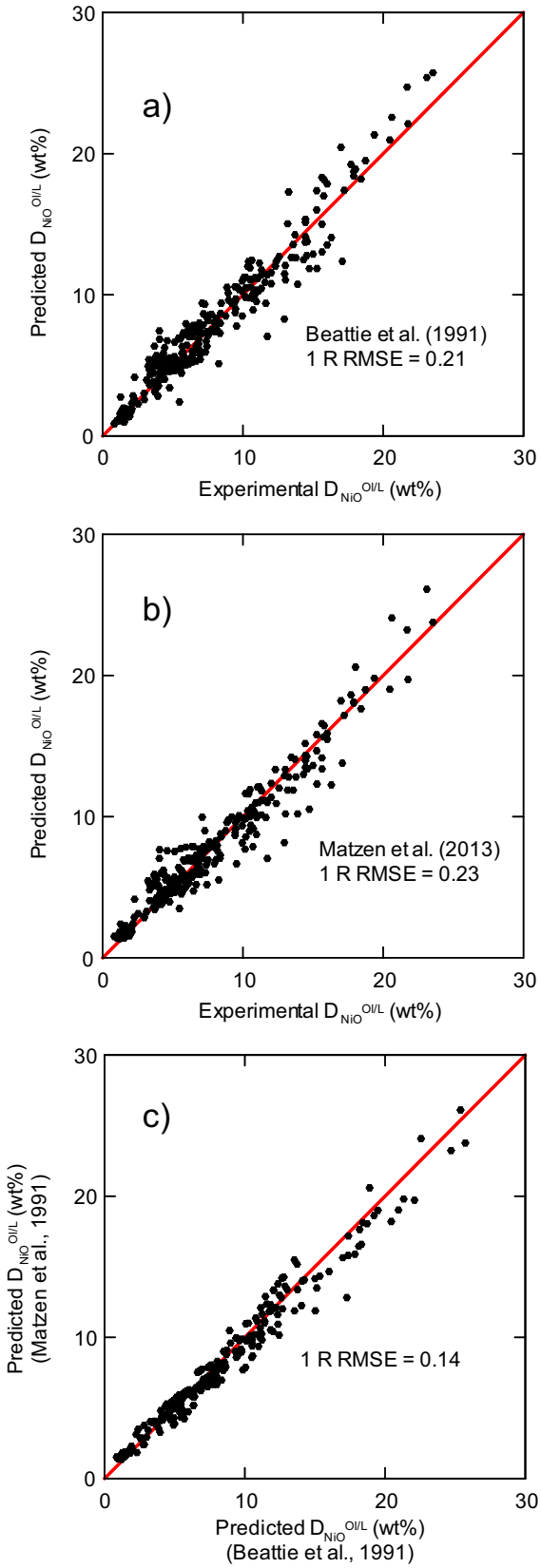

Figure 1

This is a preprint, the final version is subject to change, of the American Mineralogist (MSA)
Cite as Authors (Year) Title. American Mineralogist, in press.
(DOI will not work until issue is live.) DOI: http://dx.doi.org/10.2138/am-2016-5538

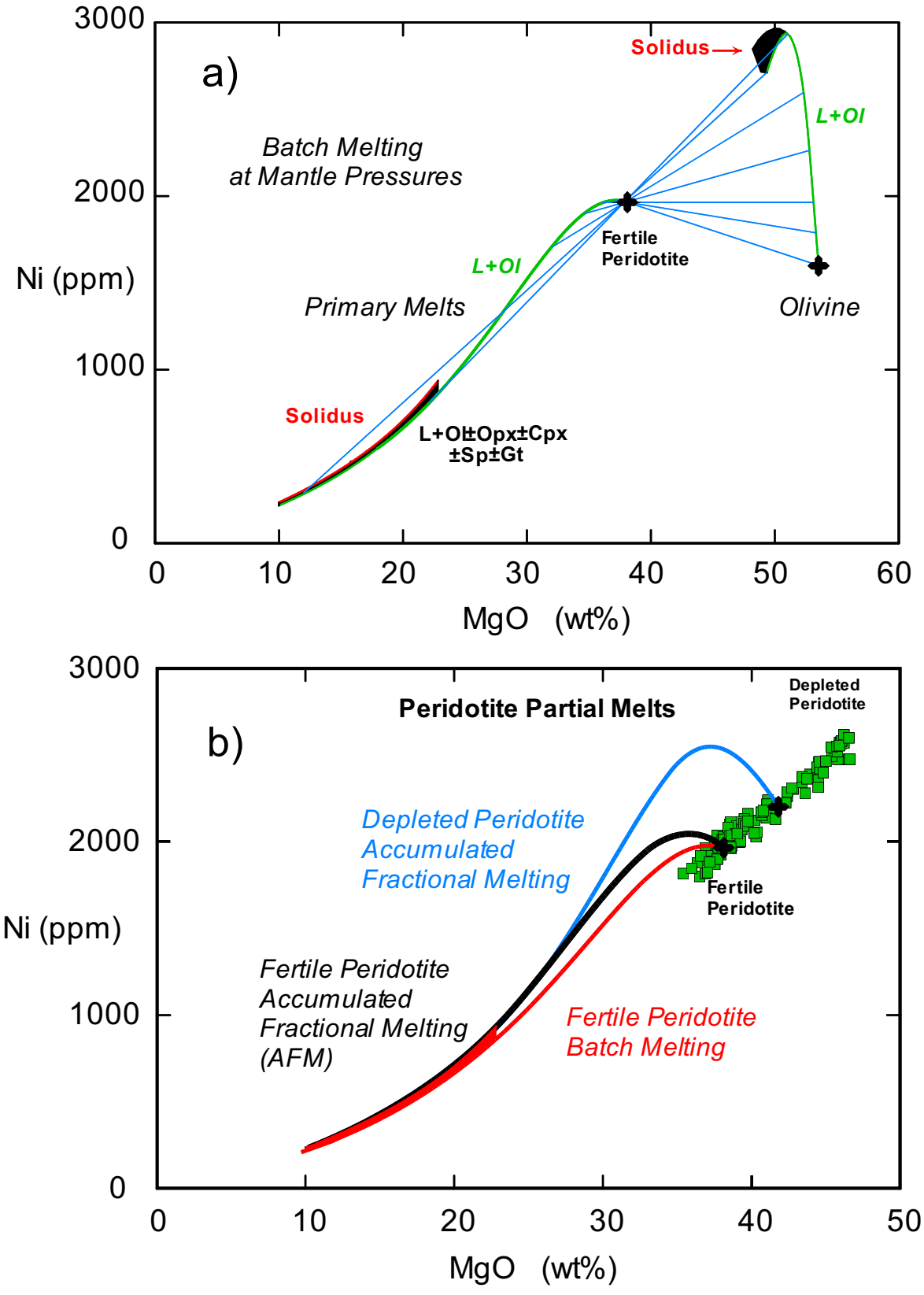

Figure 2

This is a preprint, the final version is subject to change, of the American Mineralogist (MSA)
Cite as Authors (Year) Title. American Mineralogist, in press.
(DOI will not work until issue is live.) DOI: http://dx.doi.org/10.2138/am-2016-5538

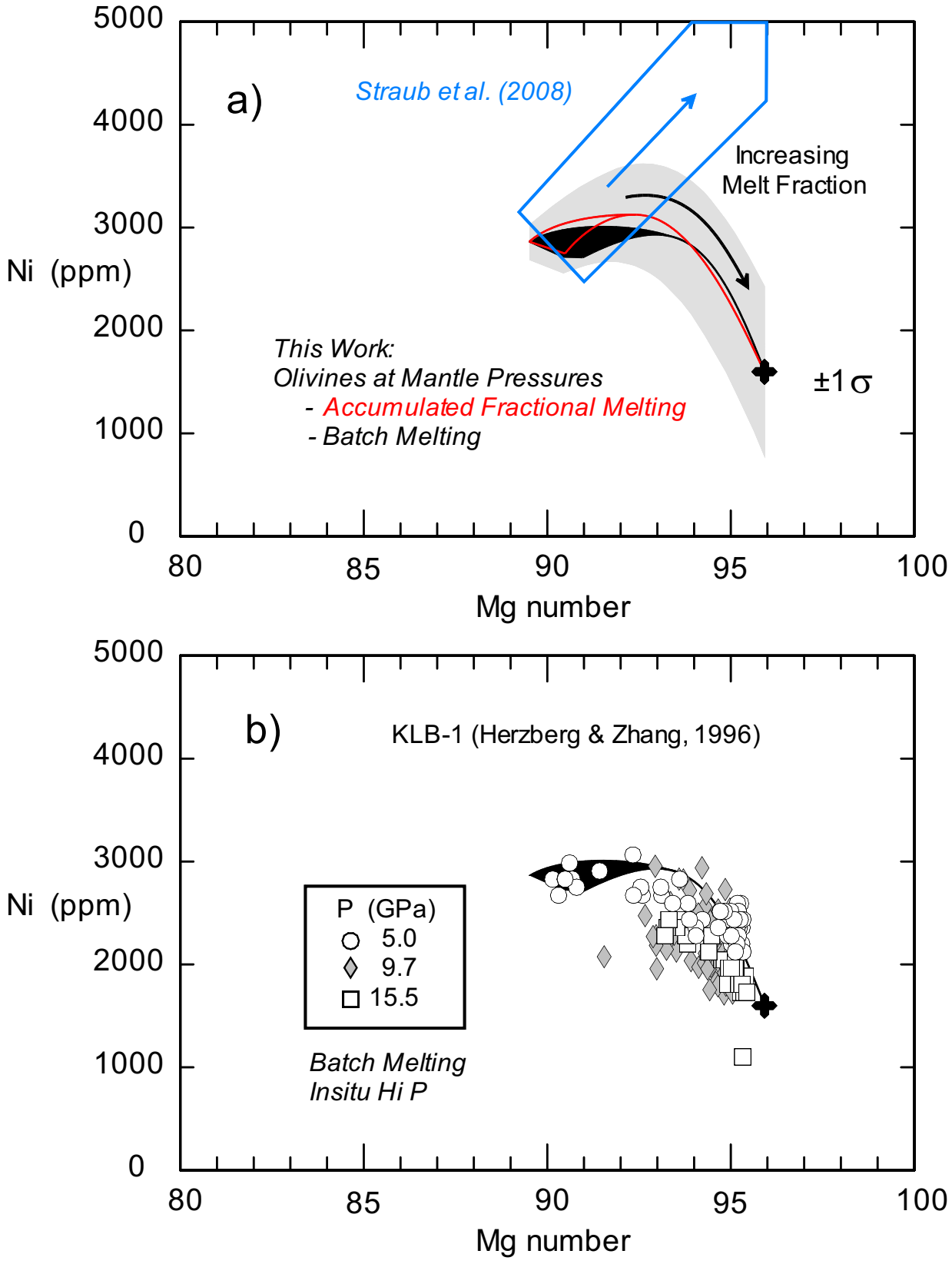

Figure 3

This is a preprint, the final version is subject to change, of the American Mineralogist (MSA)
Cite as Authors (Year) Title. American Mineralogist, in press.
(DOI will not work until issue is live.) DOI: http://dx.doi.org/10.2138/am-2016-5538

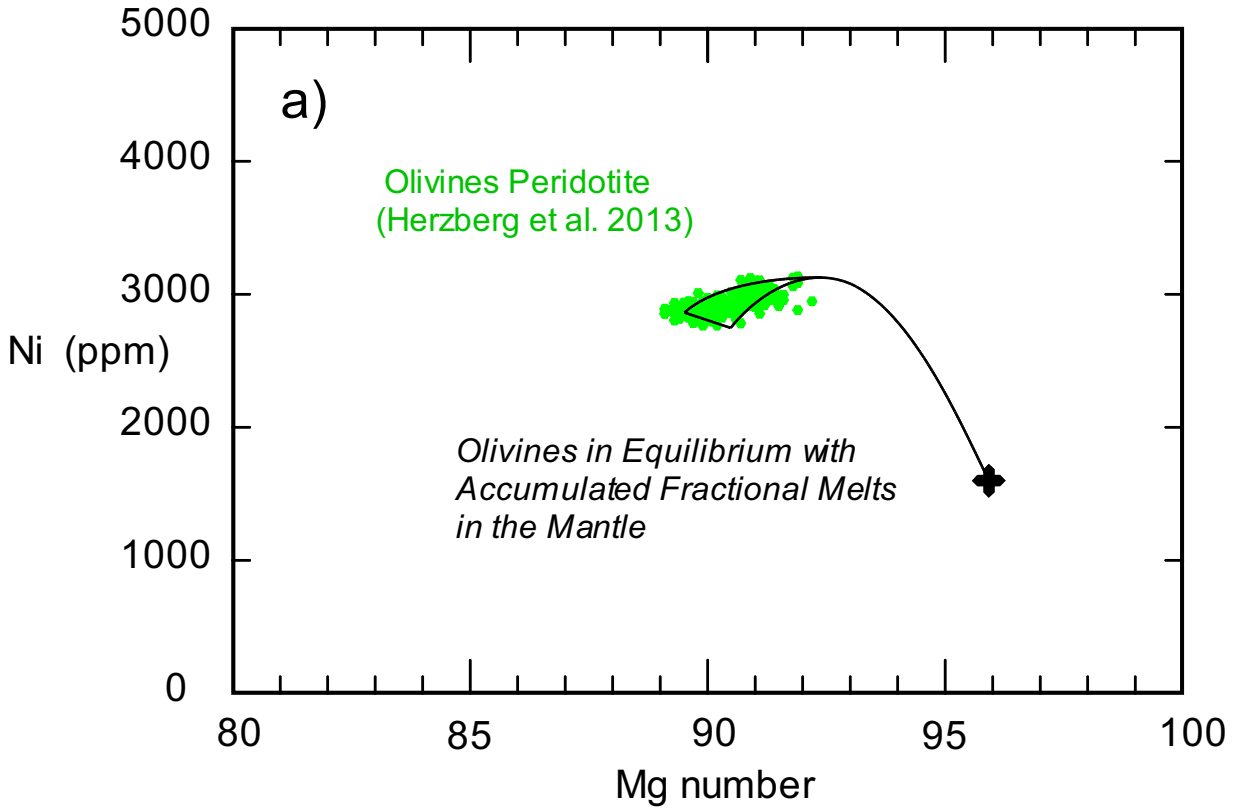

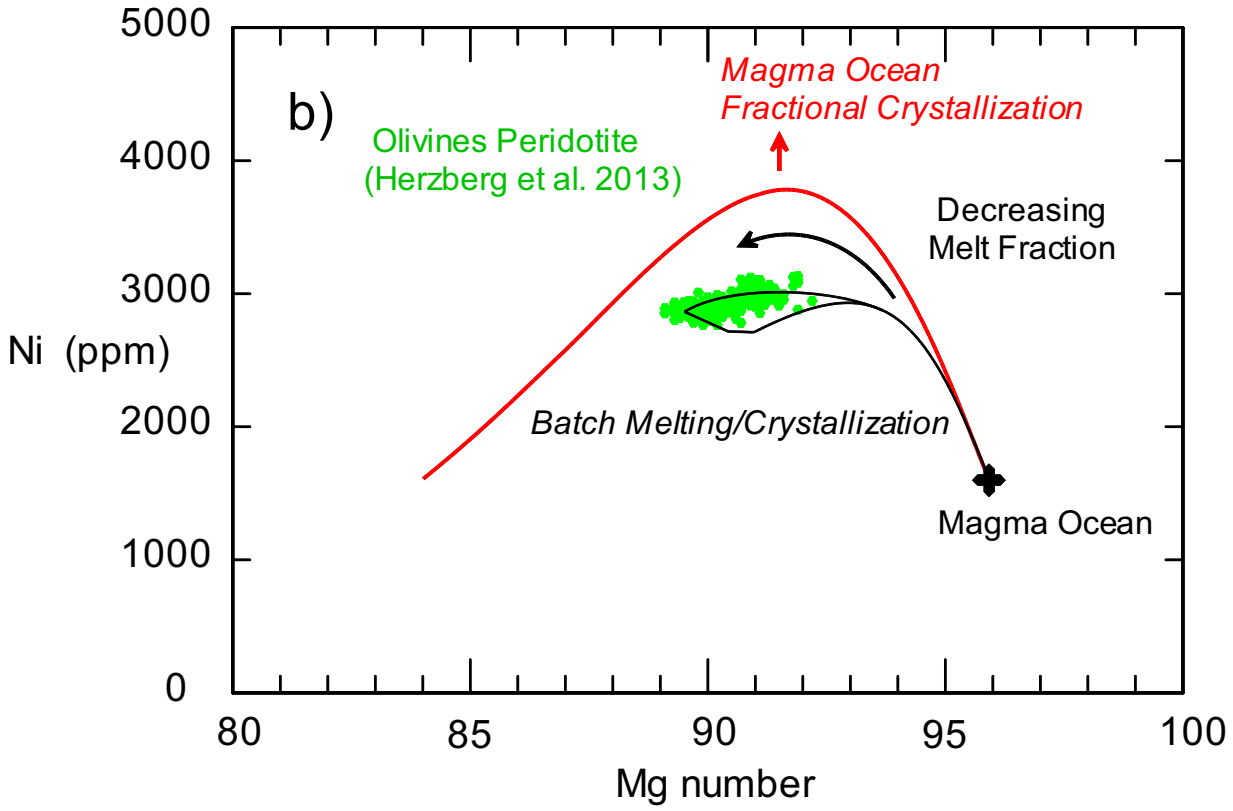

Figure 4

This is a preprint, the final version is subject to change, of the American Mineralogist (MSA)
Cite as Authors (Year) Title. American Mineralogist, in press.
(DOI will not work until issue is live.) DOI: http://dx.doi.org/10.2138/am-2016-5538

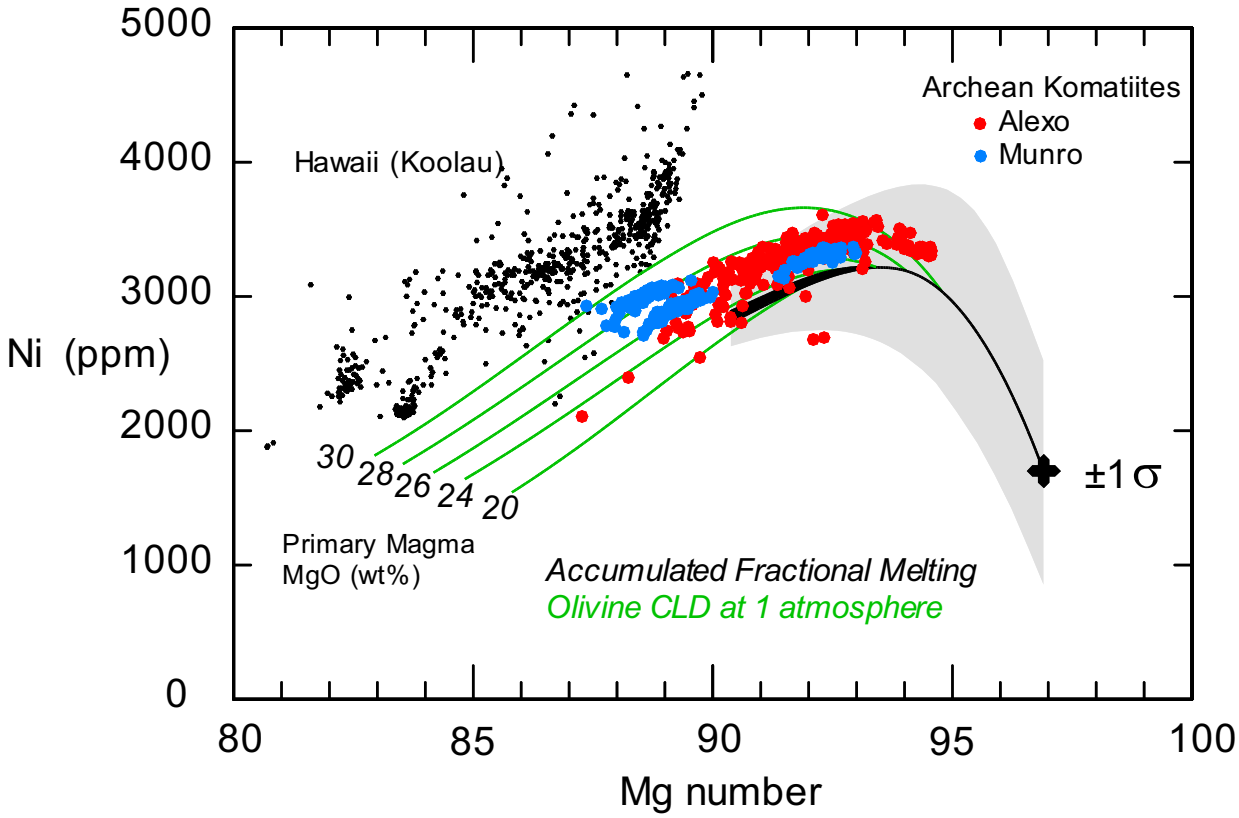

Figure 5

This is a preprint, the final version is subject to change, of the American Mineralogist (MSA)
Cite as Authors (Year) Title. American Mineralogist, in press.
(DOI will not work until issue is live.) DOI: http://dx.doi.org/10.2138/am-2016-5538

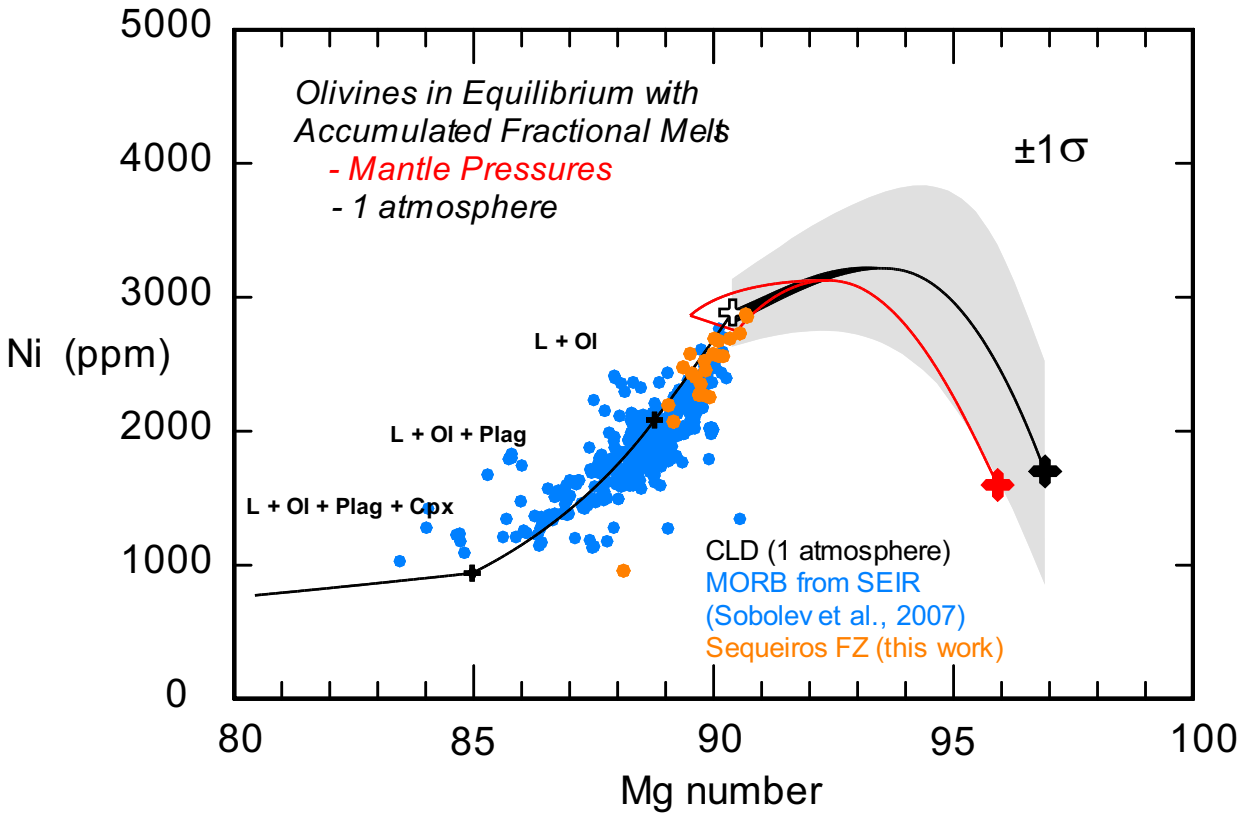

Figure 6

This is a preprint, the final version is subject to change, of the American Mineralogist (MSA)
Cite as Authors (Year) Title. American Mineralogist, in press.
(DOI will not work until issue is live.) DOI: http://dx.doi.org/10.2138/am-2016-5538

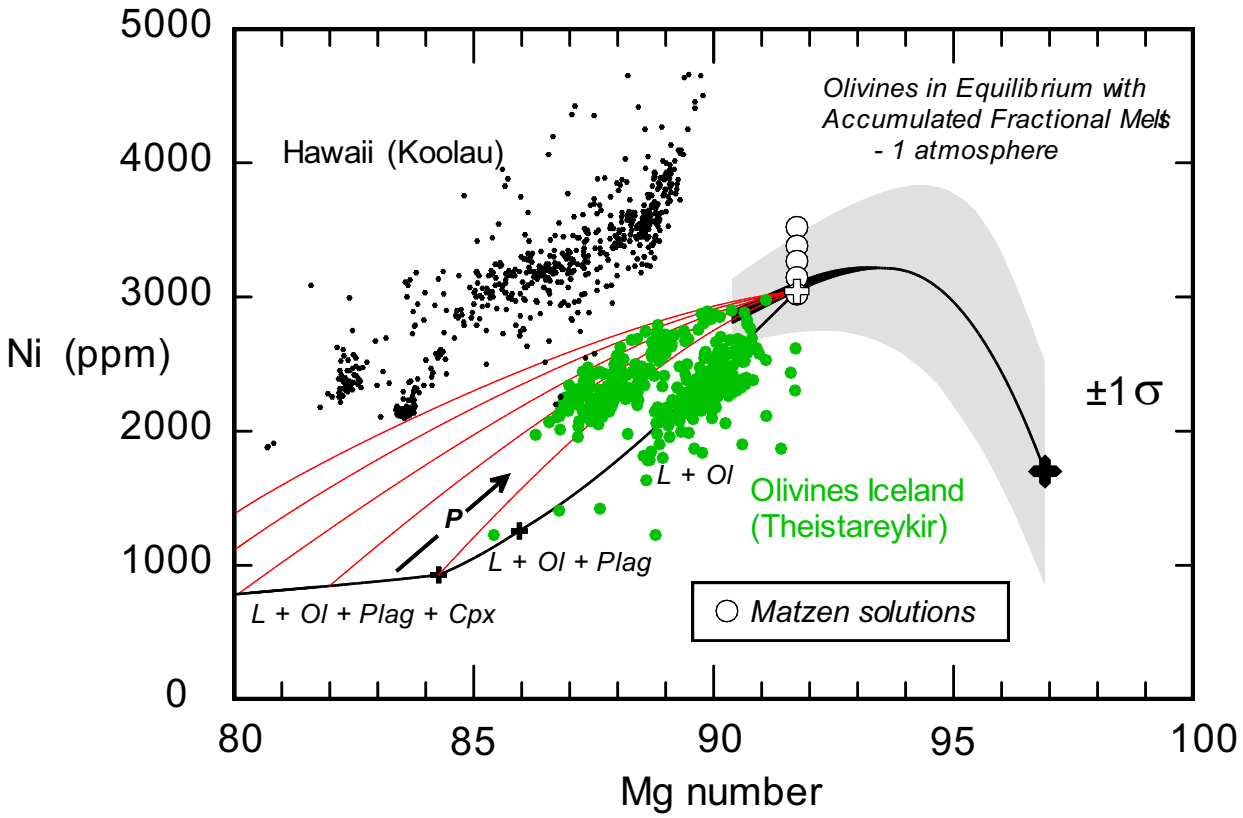

Figure 7

This is a preprint, the final version is subject to change, of the American Mineralogist (MSA)
Cite as Authors (Year) Title. American Mineralogist, in press.
(DOI will not work until issue is live.) DOI: http://dx.doi.org/10.2138/am-2016-5538

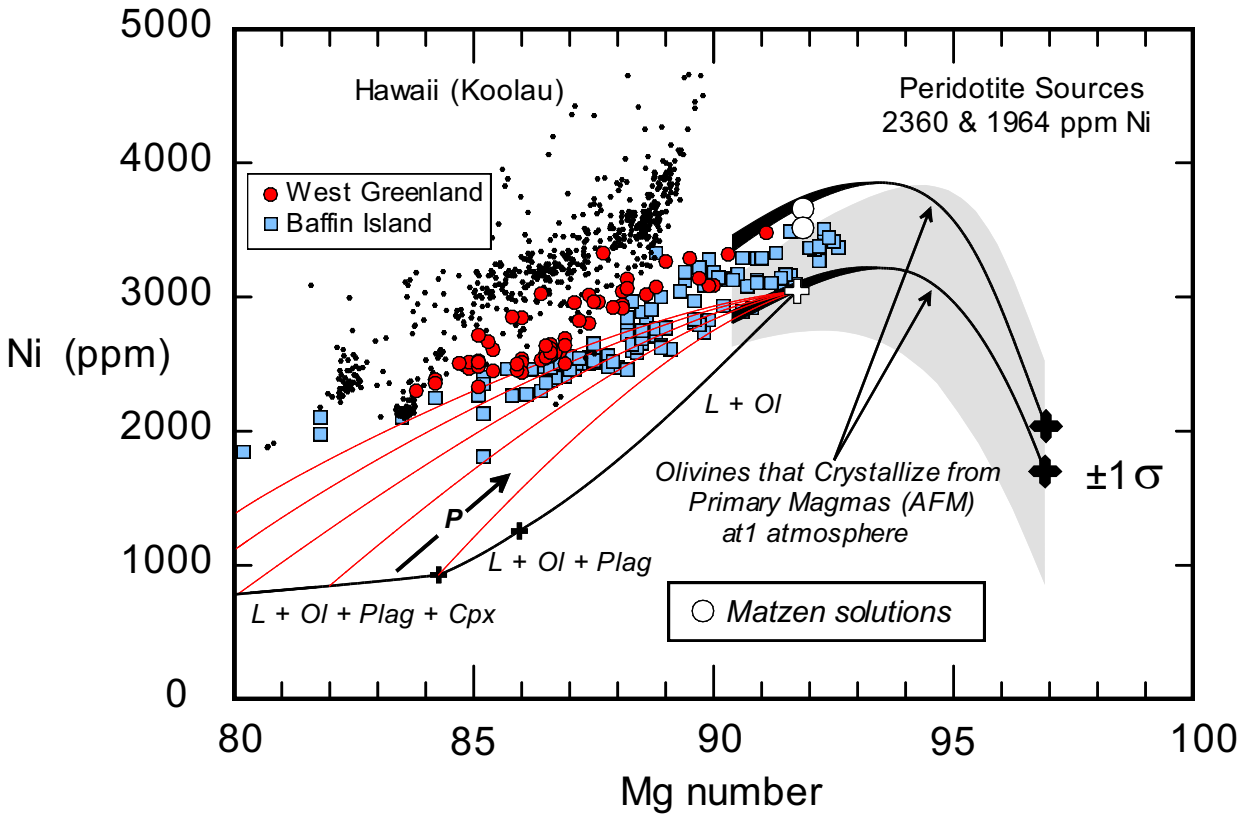

Figure 8

This is a preprint, the final version is subject to change, of the American Mineralogist (MSA)
Cite as Authors (Year) Title. American Mineralogist, in press.
(DOI will not work until issue is live.) DOI: http://dx.doi.org/10.2138/am-2016-5538

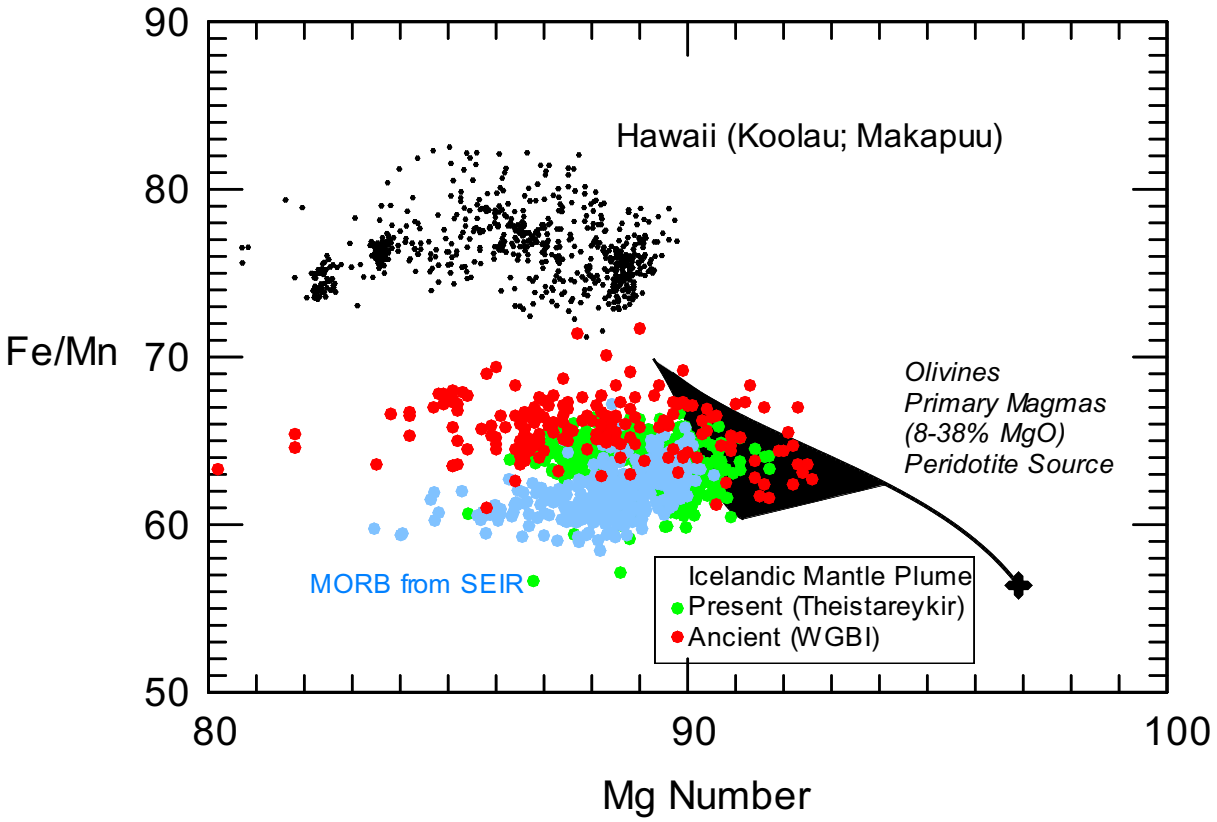

Figure 9

This is a preprint, the final version is subject to change, of the American Mineralogist (MSA)
Cite as Authors (Year) Title. American Mineralogist, in press.
(DOI will not work until issue is live.) DOI: http://dx.doi.org/10.2138/am-2016-5538

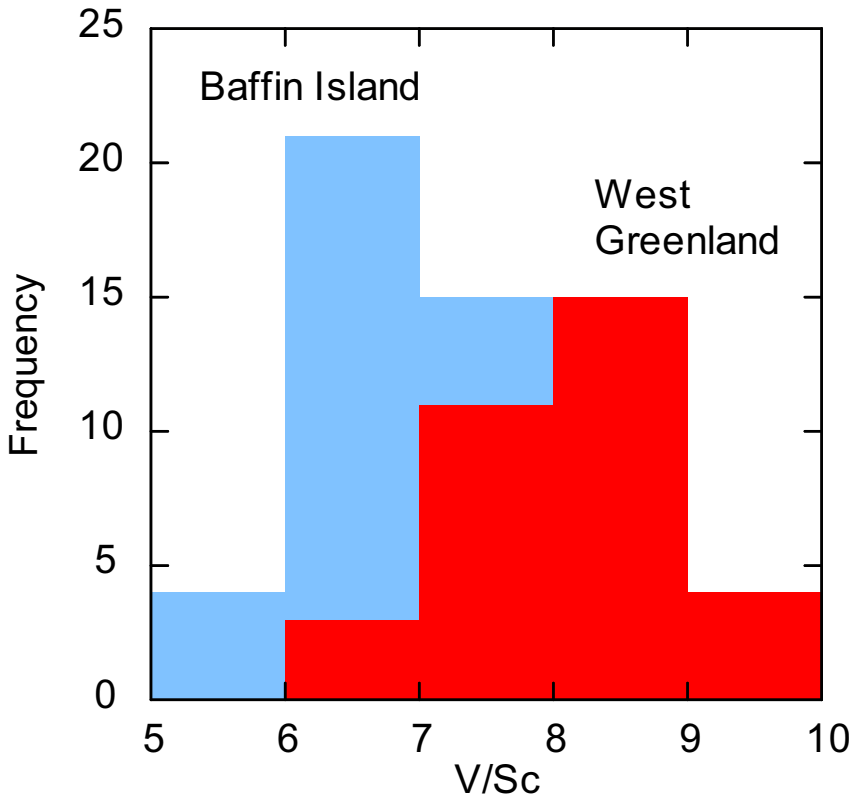

Figure 10

This is a preprint, the final version is subject to change, of the American Mineralogist (MSA)
Cite as Authors (Year) Title. American Mineralogist, in press.
(DOI will not work until issue is live.) DOI: http://dx.doi.org/10.2138/am-2016-5538

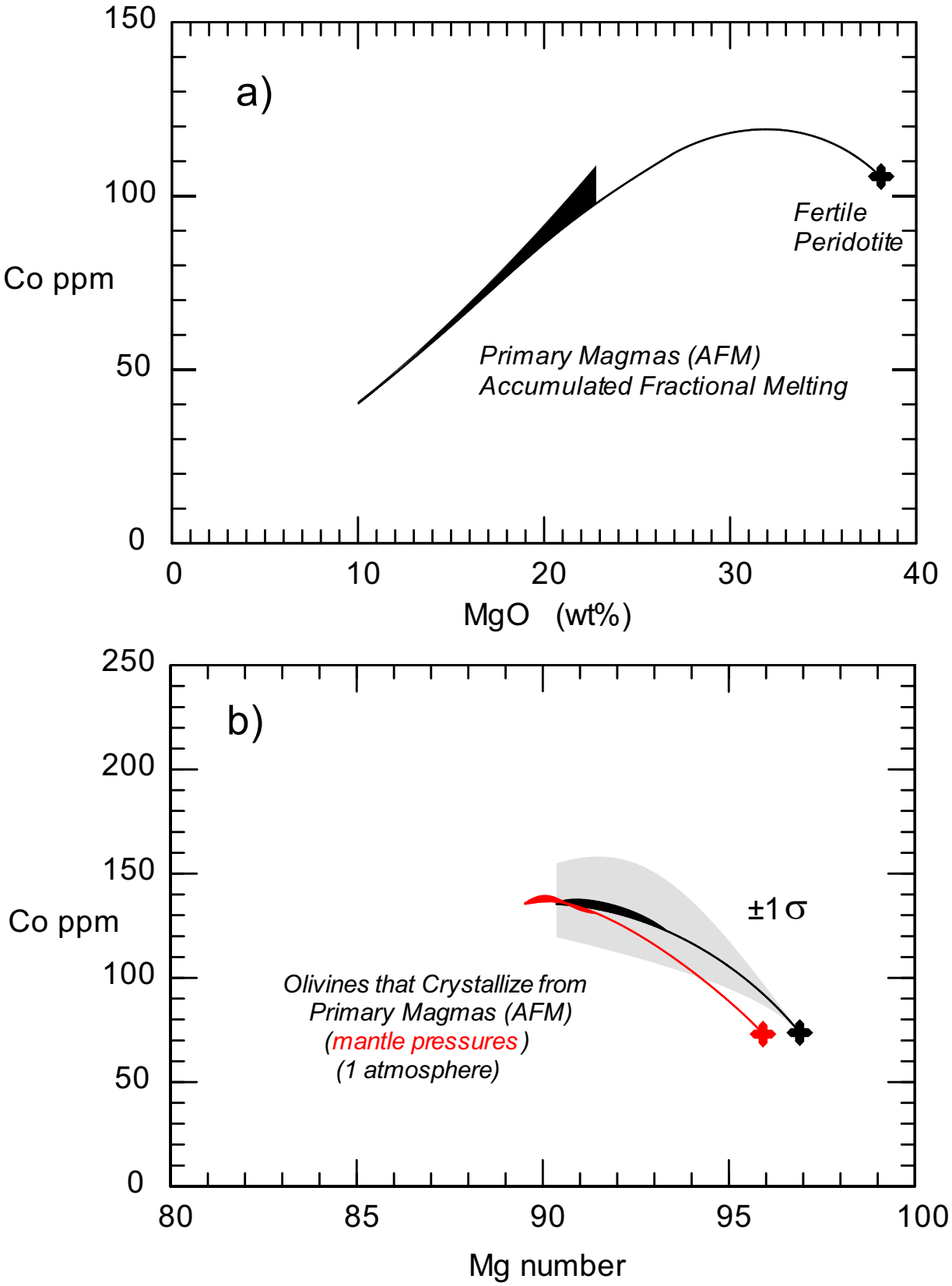

Figure 11

This is a preprint, the final version is subject to change, of the American Mineralogist (MSA)
Cite as Authors (Year) Title. American Mineralogist, in press.
(DOI will not work until issue is live.) DOI: http://dx.doi.org/10.2138/am-2016-5538

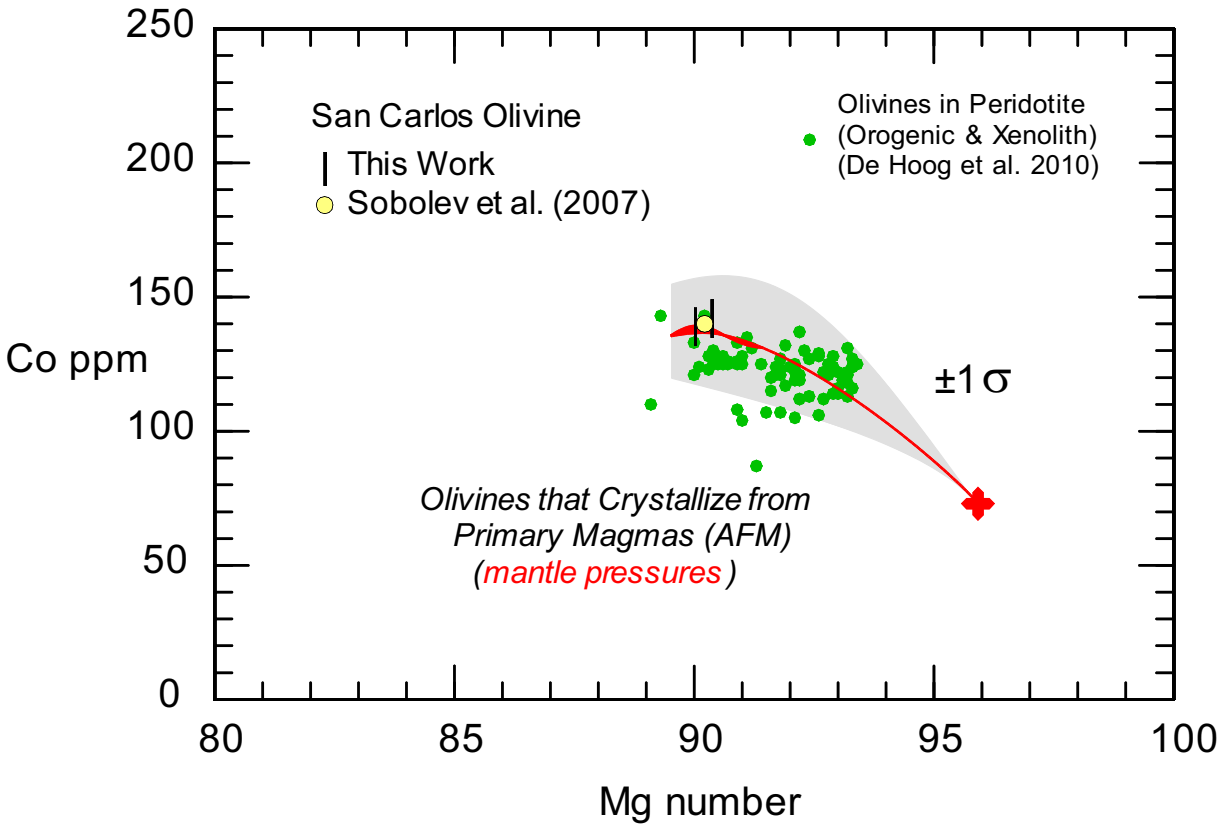

Figure 12

This is a preprint, the final version is subject to change, of the American Mineralogist (MSA)
Cite as Authors (Year) Title. American Mineralogist, in press.
(DOI will not work until issue is live.) DOI: http://dx.doi.org/10.2138/am-2016-5538

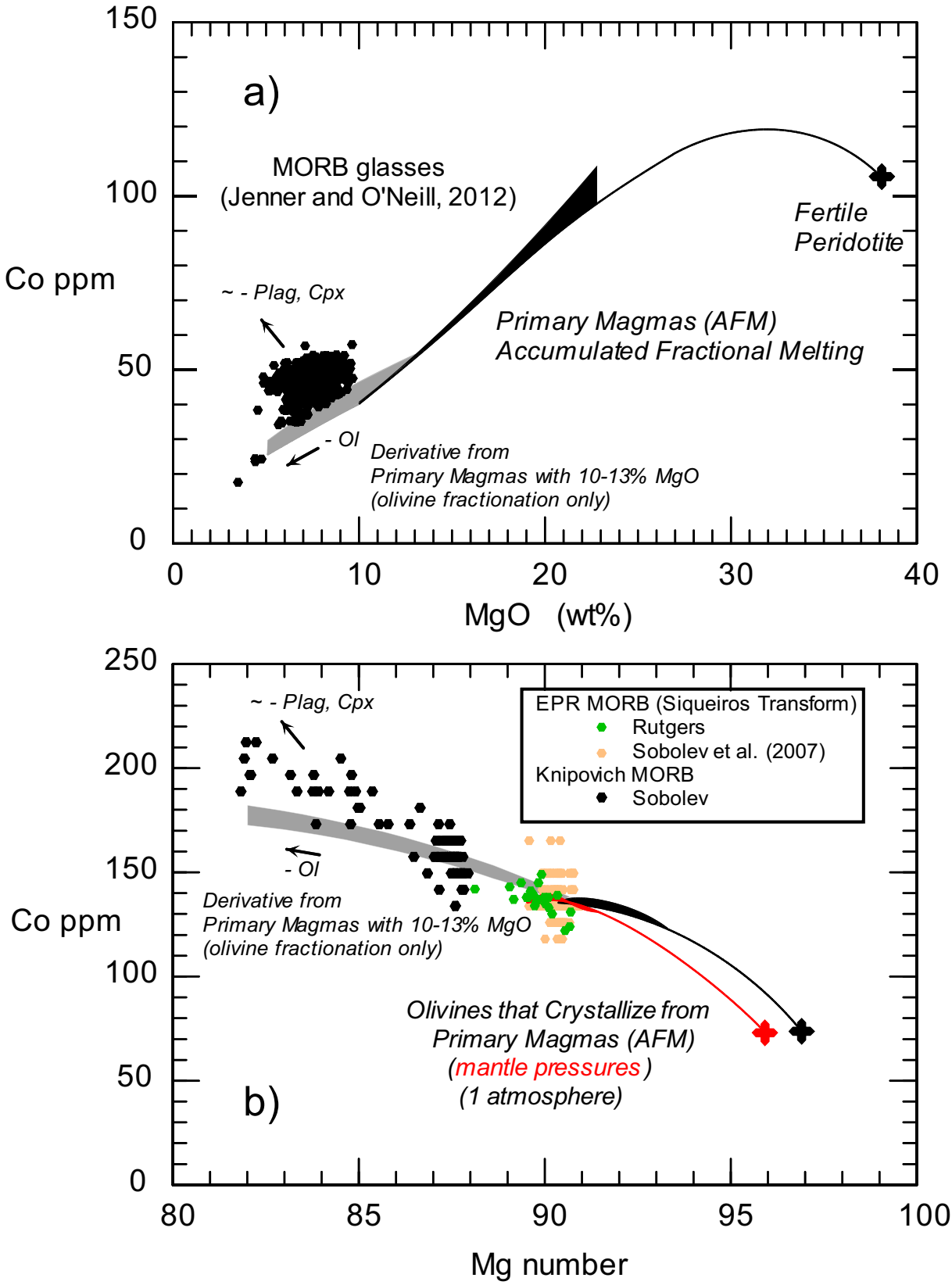

Figure 13

This is a preprint, the final version is subject to change, of the American Mineralogist (MSA)
Cite as Authors (Year) Title. American Mineralogist, in press.
(DOI will not work until issue is live.) DOI: http://dx.doi.org/10.2138/am-2016-5538

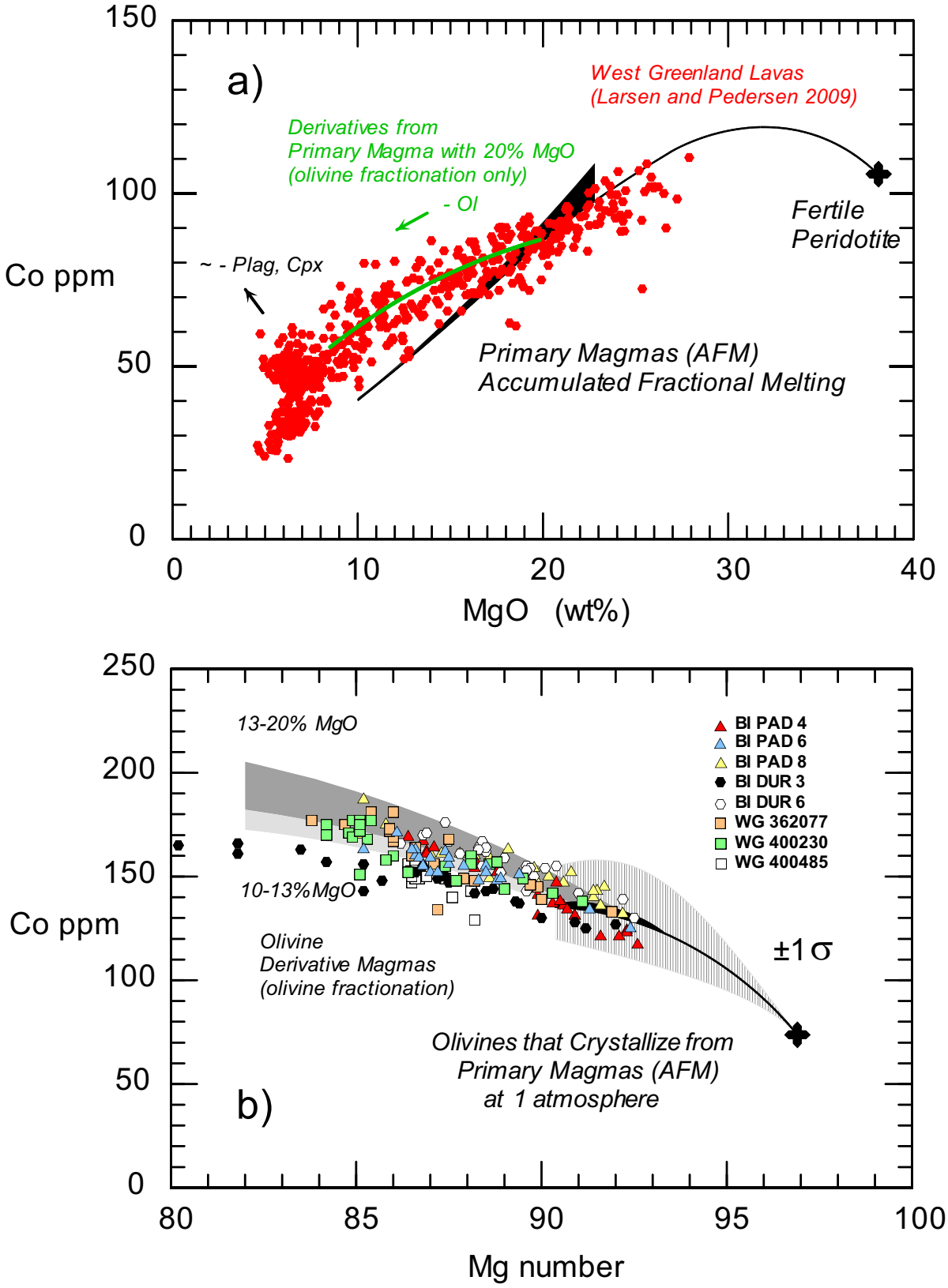

Figure 14